bericht

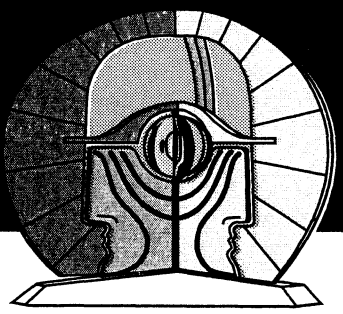

PTB-Th-2
Braunschweig, April 2005

Gerhard Schuster, Albrecht Hoffmann,
and Dieter Hechtfischer

PTB-96,
the ultra-low temperature scale of PTB

Physikalisch-Technische Bundesanstalt

Thermodynamik
PTB-Th-2

Braunschweig, April 2005

Gerhard Schuster, Albrecht Hoffmann, and Dieter Hechtfischer

PTB-96, the ultra-low temperature scale of PTB

ISSN ist beantragt
ISBN 3-86509-310-8

PTB-96, the ultra-low temperature scale of PTB

G. Schuster, A. Hoffmann, and D. Hechtfischer

Physikalisch-Technische Bundesanstalt, Abbestraße 2-12, 10587 Berlin, Germany

Abstract. The establishment of the ultra-low temperature scale at PTB in the range from 1 mK to 1 K, and its transfer to the ^{3}He melting pressure equation, is described. The temperature scale, which has been constructed with magnetic thermometry to obtain a smooth pressure-temperature relation over a wide range, ultimately relies on primary noise thermometry. The construction and verification of the scale is discussed, and a comparison with other temperature scales is presented.

Contents

1. Introduction 1

2. Construction of the reference scale 2

3. Traceability of ^{3}He melting pressures to the PTB primary standard 5

Pressure balance as a primary standard 5
International comparisons 7
Secondary pressure standard 8
Calibration of the melting pressure sensor 10
Uncertainty compilation 13

4. Confidence checks of PTB-96 16

5 Verification of PTB-96 with noise thermometry 18

6. Thermodynamic consistency 26

7. Temperature scale comparisons 31

8. Conclusions 34

References 35

1. Introduction

The relation between pressure and temperature of melting ^{3}He is well suited as a carrier of an ultra-low temperature scale due to its excellent reproducibility, its wide temperature range, and its high temperature sensitivity. Since no other thermometer exhibits all these virtues between 1 mK and 1 K, the Comité International des Poids et Mesures adopted it as Provisional Low Temperature Scale PLTS-2000 [1] to extend the International Temperature Scale ITS-90.

Although melting ^{3}He resides on a firm thermodynamic basis, the Clausius-Clapeyron equation, its temperature can be calculated only incompletely from pressure. It is therefore necessary to determine the relationship by measurement and to establish an empirical equation. This equation is then eminently useful to reproduce previous measurement results, to relate measurements made in different temperature regions, to compare different thermometers without actually operating them, and to calibrate practical thermometers. These are essentially the functions of a temperature scale.

This paper describes the work done at PTB to establish the ^{3}He pressure-temperature equation in the concrete form of the temperature scale PTB-96 [2, 3]. The main thermometer used to provide its temperature basis is the noise thermometer with its indisputable thermodynamic fundament. It implies that the noise voltage at the terminals of a resistor is caused by the thermal fluctuations of the charge carriers. The noise voltage actually measured using a complex signal processing method, however, may be affected by parasitic noise that is coupled anywhere into the signal path. Since it would not be helpful to ignore this potential cause of systematic errors, all parasitic noise effects have to be either eliminated or corrected in the final result.

Thermal noise does not differ from white noise due to other sources and therefore can not be easily discriminated from parasitic noise. Although there are sources that can be identified by parameter variation of the signal processing, this is not feasible for noise that is already mixed with the thermal noise before any processing begins. The only way to identify such interference is to take the temperature variation of the deviation of the uncorrected noise temperatures, assuming that there are no parasitic noise sources, from temperatures obtained with another thermometer as a guide. The thermometers employed for this purpose were magnetic thermometers because of their predictable variation over wide temperature ranges. They make use of the susceptibility of a cerium magnesium nitrate (CMN) single crystal at high and platinum nuclear magnetic resonance (NMR) at low temperatures. The practical method was to establish a ^{3}He melting pressure equation which represents the CMN temperatures above 40 mK and NMR temperatures below 50 mK where the crossover is smoothed with the help of the expected temperature dependence of ^{3}He melting pressure itself. Originally, the only purpose of this procedure was to take advantage of the excellent reproducibility and ease of measurement offered by the melting pressure. Therefore, the underlying reference temperature scale had no *a priori* uncertainty specification. Its only purpose was to reproduce CMN and NMR temperatures, and it gained thermodynamic significance only through comparison with the temperatures obtained afterwards from the noise thermometer.

It turned out later that this reference scale was in excellent agreement with the temperatures from the noise thermometer (including the model used for error correction) within its uncertainty limits. Thus the thermodynamic value of the reference scale relies completely on the noise thermometer and, in this sense, is based on noise thermometry. The coincidence of the reference scale with the noise scale may be interpreted as an indication that the major features of the ^{3}He melting curve have been taken into account. Since no significant systematic deviations were observed, the reference scale could be maintained without correction as PTB-96. Its temperatures will be designated by the letter T throughout this paper.

Due to the statistical measurement principle with a finite sampling rate, application of the noise thermometer is extremely time consuming. Therefore, the reference scale was verified by noise thermometry only at selected points to have more time available for the reduction of the statistical uncertainty but with the option of making more measurements if required by significant deviations. The different thermometers which have contributed to the reference scale, or which have been employed for the consistency checks, are shown in figure 1 over the temperature range where they have been used.

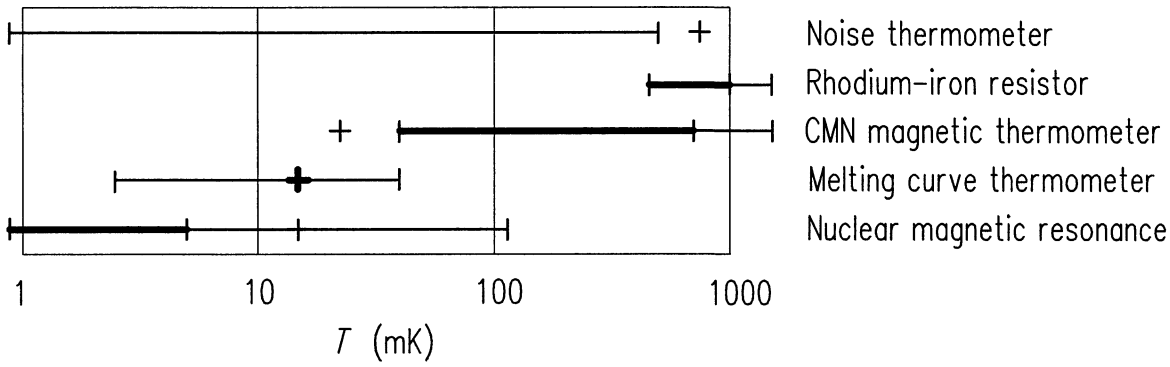

Figure 1. Thermometry employed during construction, consistency checks, and verification of the reference scale. Thick lines denote components that have directly contributed to the construction.

2. Construction of the reference scale

Magnetic thermometers, based on the Curie law, are well suited to extend a temperature scale below its definition range. It was found experimentally that an extrapolation of the NPL temperature scale T_{X1} [4] from above 1.2 K supplied an approximation of noise temperatures down to 50 mK within some tenth of a percent [5], provided a magnetic thermometer with a high purity single crystal sphere of CMN is used with the Weiss constant according to [6]. For easier access in the dilution refrigerator range below 0.7 K, a rhodium-iron resistor (RIR) had been calibrated by means of this extrapolation down to 0.45 K. With a special bridge operating at low power [7], this RIR served directly as the basis for ^{3}He melting temperature measurements between 0.45 K and 1 K. The RIR was also used to calibrate the CMN single crystal thermometer between 0.45 K and 0.7 K for the temperature range extension down to 40 mK. The mutual inductance bridge [8] employed for the CMN measurements was equipped with an automatic reduction of power input to the sensor for decreasing temperature. Its lower limit of 40 mK was imposed by the intolerably slow response of the CMN single crystal.

The measurements were made using the dilution refrigerator MK1 with an experimental arrangement described in detail elsewhere [9]. Each temperature value was kept stable by means of an automatic temperature controller [10]. To avoid temperature offsets between the CMN sensor and the melting pressure sensor, they were placed in close proximity to each other but far away from the temperature gradient between the heat source of the control loop and the heat sink of the refrigerator. Absence of such potential systematic error sources was checked frequently during temperature control by raising the cooling power, which increases the gradient, and watching for temperature differences. Operation at temperatures above the 0.7 K upper limit of the dilution refrigerator was made possible by transferring the function of the mixing chamber to the next stage on top of it (base plate). The lower cooling power available in this mode was still sufficient for automatic temperature control.

The melting curve equation in the range above 40 mK was obtained by fitting the pressure p as a polynomial in temperature T (weighted with temperature). The fitting residuals in fig-

ure 2 demonstrate that this polynomial is uncertain with respect to the data by about ±0.02% except for the immediate neighbourhood of the melting pressure minimum. Loops visible in the residuals are caused by the hysteresis of the melting pressure sensor that appear when measurements are made with rising and falling temperatures.

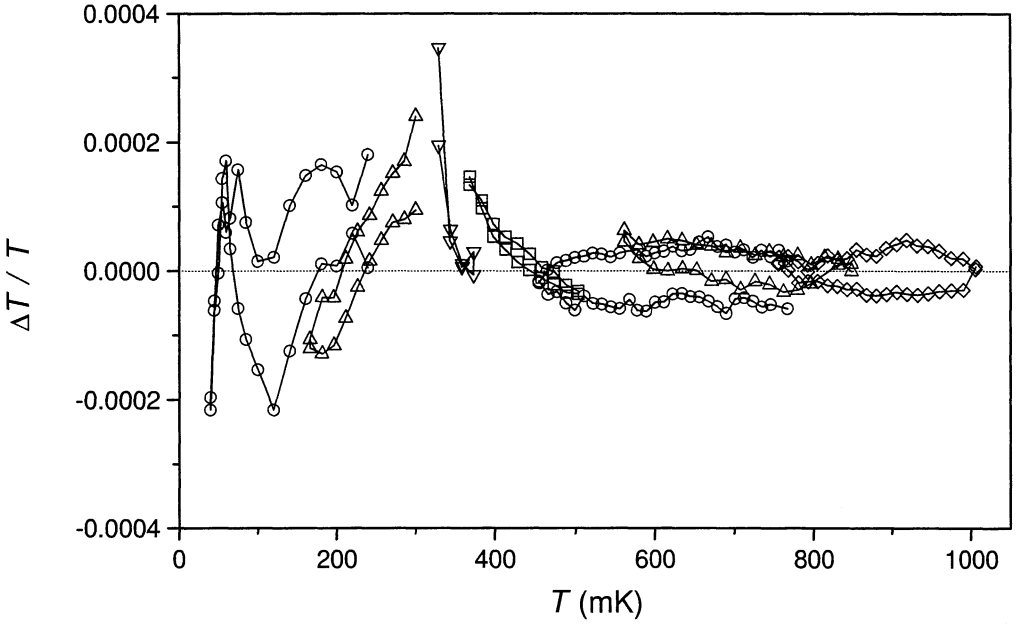

Figure 2. Relative temperature deviation of the polynomial from the RIR and CMN thermometer data.

Further extension of the reference scale was made with platinum nuclear magnetic resonance (NMR) [11]. Due to the low sensitivity of this thermometer at the junction, however, a direct calibration would have caused a loss of precision. Therefore the melting pressure polynomial itself was used to continue the temperature scale down to the point where the NMR thermometer is competitive. The central extrapolated reference temperature for the extension of the scale was selected to be 15 mK. This point is a practical starting temperature for the nuclear demagnetisation refrigerator MK2, which was required to reach the range below 5 mK anyway. It should be emphasised that such an extrapolation is primarily a practical approach, which is justified by the intention to measure and correct the reference scale afterwards with primary thermometry. The procedure is working because the melting pressure has no strong curvature in this temperature region due to the fact that its slope is governed there by the nearly temperature independent solid ^{3}He entropy. An indication, that this extrapolation would need only small corrections, was a temperature for the ^{3}He superfluid (A) transition of 2.67 mK obtained from the measured pressure using the polynomial instead of the true PTB-96 value 2.41 mK.

The next step was to determine the corrections required for extension of the scale to below 15 mK. This was accomplished by calibrating the NMR thermometer, which is supposed to follow a pure Curie law [12], at 15 mK and measuring the temperature difference below 5 mK with respect to the extrapolated melting temperature. Due to the growing temperature dependence of the solid ^{3}He entropy, the melting pressure deviates by increasing powers in $1/T$ from a linear relationship in this region, which suggests a polynomial of the same shape for the correction function. Experimentally, the measured temperature difference, taken as a function of $1/T$, is a smooth relation that can be well approximated by a third order polynomial as illustrated in figure 3.

This temperature correction has been combined with the melting pressure polynomial obtained from above 40 mK to generate a pressure versus temperature table with logarithmic

spacing over the complete range between 0.88 mK and 1000 mK as basis for the final fitting procedure. The far reaching $1/T$ dependence, which still influences data above 40 mK, has been taken into account by a small shift in such a way as to preserve the combined value at 15 mK. Final fitting was made with explicit weighting proportional to T. The logarithmic data spacing provided implicit weighting at the lowest temperatures. Simultaneous weighting at both ends was necessary to avoid oscillations of the fitting polynomial at either boundary, and also supplied less weight to the region between 5 mK and 40 mK, where experimental temperatures were not available.

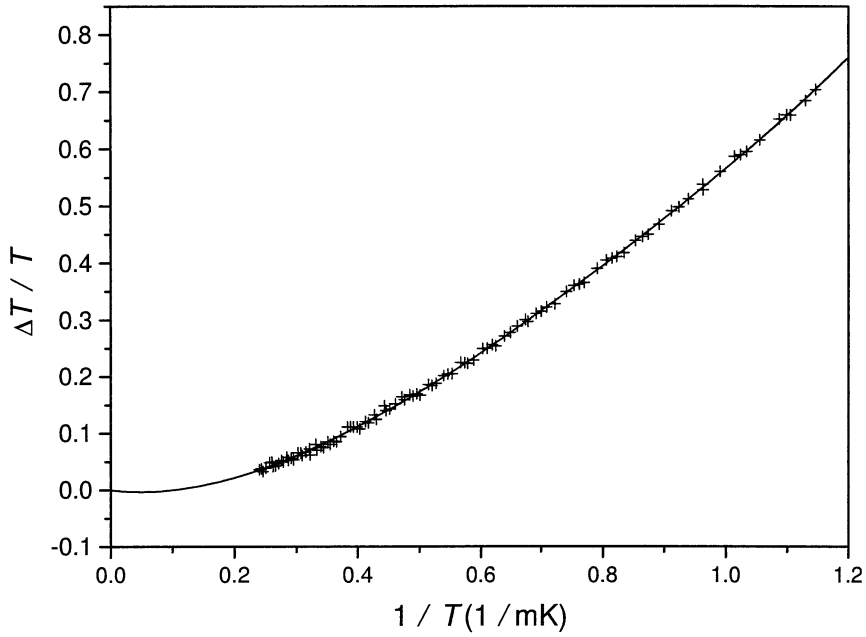

Figure 3. Relative difference between NMR and extrapolated melting temperatures. Continuous line denotes fit polynomial. Scatter of the individual data points is of the order of ±10 μK (root of the mean of squares).

The result, presented in table 1, is a melting pressure equation which is continuous and smooth between 0.88 mK and 1 K. Its deviation from the original temperatures is generally of the order of the scatter of the experimental data points.

Table 1. PTB equation for the temperature dependence of ^{3}He melting pressure (PTB-96) [3].

$$p = \sum_{i=-3}^{+9} a_i T^i$$

with p (MPa), T (K), and the coefficients a_i specified below.

a_{-3} =	-7.2175164	· 10^{-13}
a_{-2} =	2.9055958	· 10^{-9}
a_{-1} =	-5.0441980	· 10^{-6}
a_0 =	3.4461924	· 10^{0}
a_1 =	-4.4127628	· 10^{0}
a_2 =	1.5401113	· 10^{1}
a_3 =	-3.5780818	· 10^{1}
a_4 =	7.1567462	· 10^{1}
a_5 =	-1.0429605	· 10^{2}
a_6 =	1.0524591	· 10^{2}
a_7 =	-6.9301578	· 10^{1}
a_8 =	2.6659433	· 10^{1}
a_9 =	-4.5298212	· 10^{0}

3. Traceability of ^{3}He melting pressures to the PTB primary standard

The constructive details of the melting pressure sensor have been described elsewhere [9]. A required pressure resolution of the sensor of about 1 Pa in the range from 2.9 to 4.0 MPa means that the capacitor plate deflection has to be stable and reproducible by about $2 \cdot 10^{-12}$ m during its operation. Therefore, the metal parts are permitted to perform only elastic movements against each other at changing stress, even though they are screwed together, and the capacitor plates are cemented in place to maintain insulation. These mechanical requirements for the construction are attainable in the temperature interval of 1 K where ^{3}He melting pressure thermometry is applicable. It is helpful, however, to reduce strains before using the sensor by changing the pressure over the working range repeatedly to relocate all components into a stable position. To avoid build-up of further strain, the temperature should not exceed 1.5 K after pressure calibration. In addition, the sensor should be checked in regular intervals to protect the calibration against sensor drifts and jumps of up to 100 Pa. Although such shifts cause only linear deviations with sufficient accuracy, they could compromise the measurement quality if they remain unnoticed.

Conditions for measurement of the ^{3}He melting pressures are different depending on whether they are intended to determine the melting pressure equation $p = f(T)$, or whether the equation is already known and only the sensor has to be calibrated. In the first case, the pressure calibration must be traceable to the primary pressure standard, and a head correction must be determined from the density distribution of the ^{3}He liquid or gas column [9]. During the melting pressure measurements a plug of solid ^{3}He seals the sensor volume. The pressure fixed points on the ^{3}He melting pressure curve or superconductive temperature reference points can then serve for checking the pressure stability. In the second case, the traceability of the pressure calibration is not required. It is sufficient, that the reference standard has a linear dependence on pressure. Then the nonlinearity of the sensor can be measured, and the linear part corrected at the ^{3}He fixed points. This condition is satisfied as well with the pressure balance as with the quartz oscillator pressure transducer used for the calibrations. In practice, the pressure sensor is usually calibrated in a two-step process. First, a pressure transducer is calibrated using a pressure balance, and second the melting pressure sensor is calibrated with the pressure transducer. This procedure was chosen to avoid contamination of the ^{3}He filling.

Pressure balance as a primary standard.

A commercial gas-operated oil-lubricated piston-cylinder assembly with an effective area of 1 cm² was used as pressure standard. The piston-cylinder unit and the load weights are part of the model 5200 of the manufacturer Desgranges & Huot. The measuring system, serial no. 3428, is identical with two other such systems in the pressure laboratory of PTB, and was employed together with these systems to realise the PTB pressure standard during the period from 1989 to 1997. The measuring system and the set of weights were manufactured according to the request of the highest precision class (S2) of the manufacturer. The manufacturer calibration of the piston area (0.980492 cm^2) is derived from the standards of the LNE (Laboratoire National d'Essais, France) and is specified with the relative uncertainty $\pm 4 \cdot 10^{-5}$. The masses have been adjusted with the relative uncertainty $\pm 2 \cdot 10^{-5}$ to their nominal value. These adjustments were made with comparison to the master standards of the French metrology service. The pressure balance is operated in an enclosure evacuated to < 0.5 Pa during the measurement, so that the air pressure corrections are avoided. The oil used for lubrication of the piston cylinders unit has low viscosity and a low vapour pressure in order not to cause any contamination of the weight pieces.

The required accuracy of the ^{3}He melting pressure determination can be achieved only by reducing the error limits to below those of the commercial calibration. Therefore the masses of the weights and the effective piston area must be determined by comparison with the PTB standards and, furthermore, the local acceleration of gravity at the place of the pressure balance must be measured.

The acceleration of gravity was measured by the Institut für Geodäsie und Photogrammetrie, TU-Berlin, at three places in the building and on the Berlin area of the PTB. From the data, the acceleration of gravity at the place of the pressure balance resulted in

$$g = (9.812710 \pm 0.000004)\ \mathrm{m/s^2}.$$

The masses of the set of weights, the carrier of the weights, and the piston, were calibrated in the PTB laboratory for mass. The standard deviation was calculated from the uncertainty contributions of the mass standards, the comparison of the masses, and the air pressure correction. The uncertainty of the calibration of the 2 kg weights is ±3 mg. The masses of the weight carrier and of the piston were determined with the uncertainty of ±4 mg.

The most important detail of a pressure balance is the effective area of the piston. In the year 1989 a new pressure standard was developed in the PTB for the pressure range 0.1 to 5 MPa [13]. Our piston-cylinder system was involved in the definition of this pressure standard together with two other identically constructed systems.

The effective areas of the three piston cylinder systems were determined by comparison with the primary PTB pressure standard, a 38 m high mercury column. In addition, the effective area ratios of the three piston cylinder systems were determined from pressure comparison measurements using a 5 MPa twin pressure balance as a reliability check of the area data. Further determinations of area values were made using two 1 MPa piston-cylinder assemblies (#278, #280) whose areas were found out by dimensional measurements. The calibrations, shown in figure 4, gave an effective area of the piston-cylinder unit #3428 of

$$A_0 = (0.980517 \pm 0.000007)\ \mathrm{cm^2}.$$

with a coverage factor 1 for the uncertainty limits.

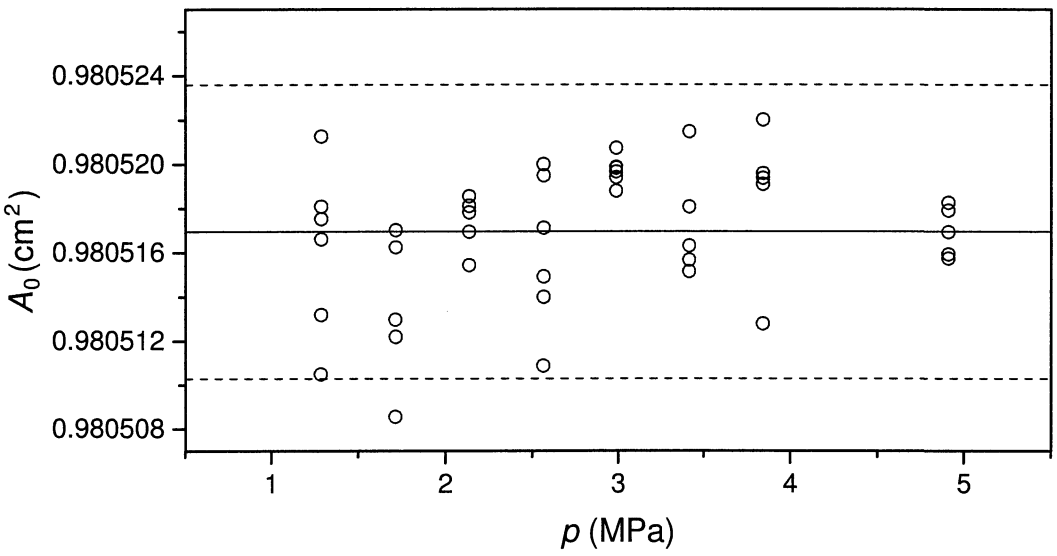

Figure 4. Calibration data of the zero-pressure effective area A_0 of pressure balance serial no. 3428, obtained from pressure measurements with the PTB high-pressure mercury column. Broken lines denote uncertainty limits. For details see [13].

In 1994, before measurements of the melting pressure equation started, the area of the piston cylinder unit was checked again. In cross-floating experiments, the area ratios were measured with the other two piston-cylinder units [14]. With the relative uncertainty of the area ratios for the two pressure balances of $\pm 2 \cdot 10^{-6}$ and $\pm 10 \cdot 10^{-6}$, respectively, the results of the calibration made in 1989 were confirmed within the uncertainty limits.

An additional comparison with the PTB pressure standards took place in conjunction with the measurements for a new primary pressure standard in the range up to 10 MPa in 1996 [15]. The new primary standard consists of three oil-operated and one gas-operated (#6222) pressure balances with the piston area of 5 cm^2. For the systems #6222 and #279, the piston areas have been measured geometrically [16]. In addition, the unit #6222 has been compared with the mercury column in the pressure range from 0.1 to 2 MPa [17, 18]. Comparison measurements were carried out between the four piston-cylinder units, using oil-gas diaphragm gauges to separate the different pressure media. The traceability of the new primary standard represented by #279 to the pressure standard in use since 1989 was made by comparison with pressure balance #3428, the one used to measure the ^{3}He melting pressure. The measurement of the piston area yielded a value below that measured with the mercury column in 1989 by $6 \cdot 10^{-6}$ cm^2, which is within the uncertainty limits of all the standards.

Caused by the results of the EUROMET Project 305 [19] carried out from 1994 to 1995, the effective area of #3428 had to be revised. In the year 1996 the comparison measurements between the system #3428 and the mercury column were repeated. The effective area was found to be (0.980509 ± 0.000007) cm^2. This value of A_0 was regarded as the final one for the piston-cylinder unit #3428 [19]. Comparison measurements of the system #279 with further similar systems [20] yielded a new consistent set of effective area values which were slightly different, for #279 by about $3 \cdot 10^{-6}$, compared to the older ones. Taking into account this shift, the value for the system #3428 would become 0.980512 cm^2.

The individual relative uncertainty of the pressure standards involved in all comparison measurements ranged from $4 \cdot 10^{-6}$ to $7 \cdot 10^{-6}$. Therefore, the calibrations performed before and after the measurements of the ^{3}He melting pressure made it sure that the changes of the value of the effective area are well within the uncertainty limits in the meantime.

International comparisons

To give a general impression of the quality of effective area calibrations, the results of several international comparison measurements are summarised that all are interrelated to the pressure balance #3428. In 1980, a comparison [21] of pressure balance standards established the equivalence of the scales of PTB and NBS (National Bureau of Standards, now NIST, USA) over the range 1 MPa to 10 MPa. The effective areas of the transfer piston-cylinder units were measured in this comparison within the relative uncertainty limits of $\pm 22 \cdot 10^{-6}$. Three units were involved at PTB whose areas were determined with the mercury column as the primary standard.

In 1991, the LNE and PTB performed a bilateral intercomparison of piston-cylinder assemblies with effective areas of 10 cm^2 [22]. The pressure balances #288 and #290 were the PTB units that had been compared already with the unit #3428 in the pressure range to 1 MPa in the year 1989. The standard deviation of the relative area data was $2 \cdot 10^{-6}$. The area data of LNE were less than those of PTB but the relative area difference of $10 \cdot 10^{-6}$ remained within the uncertainty limits of the pressure standards.

Pressure balance #3428 was also involved in two other international intercomparison measurements, in the EUROMET Project 305 [15] together with pressure standards of the LNE, and in the key comparison CCM.P-K1.c of the CCM (Consultative Committee for Mass

and Related Quantities) in the pressure range up to 1 MPa [23]. Later on the results of the EUROMET Project 305 were accepted by the CCM as key comparison EUROMET.M.P-K2 and included in the BIPM KC database [19]. In these comparisons, the area values were verified within uncertainty limits of $\pm 10 \cdot 10^{-6}$.

In a COOMET project [24], the PTB piston-cylinder assemblies #3428, #6222 and #279 were compared with units of the VNIIM (Mendeleyev Institute for Metrology, Russian Federation) and the SMU (Slovak Institute of Metrology, Slovakia) in the pressure range from 1 MPa to 3 MPa. The participants determined the piston areas of two transfer standards. Based on the results, VNIIM and SMU now are indirectly linked to the CCM key comparisons with relative discrepancies between corresponding zero-pressure effective area values of about $\pm 10 \cdot 10^{-6}$.

Since the piston cylinder system #3428 was part of the national pressure standard, many comparisons results could be used to monitor its properties over a long period of time. Therefore, the melting pressure measurements represent the PTB pressure standard with high precision, and the value of the effective area of unit #3428 is known with trustworthy relative standard uncertainty of $7 \cdot 10^{-6}$.

Secondary pressure standard

The melting pressure sensor calibrations at MK2 were not made with the pressure balance and ^{3}He gas directly but by using a commercial pressure transducer (Digiquartz model 2900-AS from Paroscientific). The pressure transducer itself was calibrated with the pressure balance using nitrogen gas to avoid contamination of the ^{3}He sensor filling by ^{4}He. The short-term stability of the calibration, the hysteresis, and primarily the linearity of the pressure transducer are quite satisfactory, as observed over a period of 10 years. Although the pressure transducer is operated in a thermostat, the long-term stability of the display (oscillator period) at low pressure (<10 Pa) was insufficient. The zero-pressure oscillation period decreased monotonously from 24.4219 µs in the year 1987 to 24.4131 µs in the year 1998. This corresponds to an offset of 24 kPa within 11 years. For every calibration, therefore, the actual value at zero pressure had to be measured and the pressure data referred to this value. The residual variation of the calibration is shown in figure 5 against the pressure balance data.

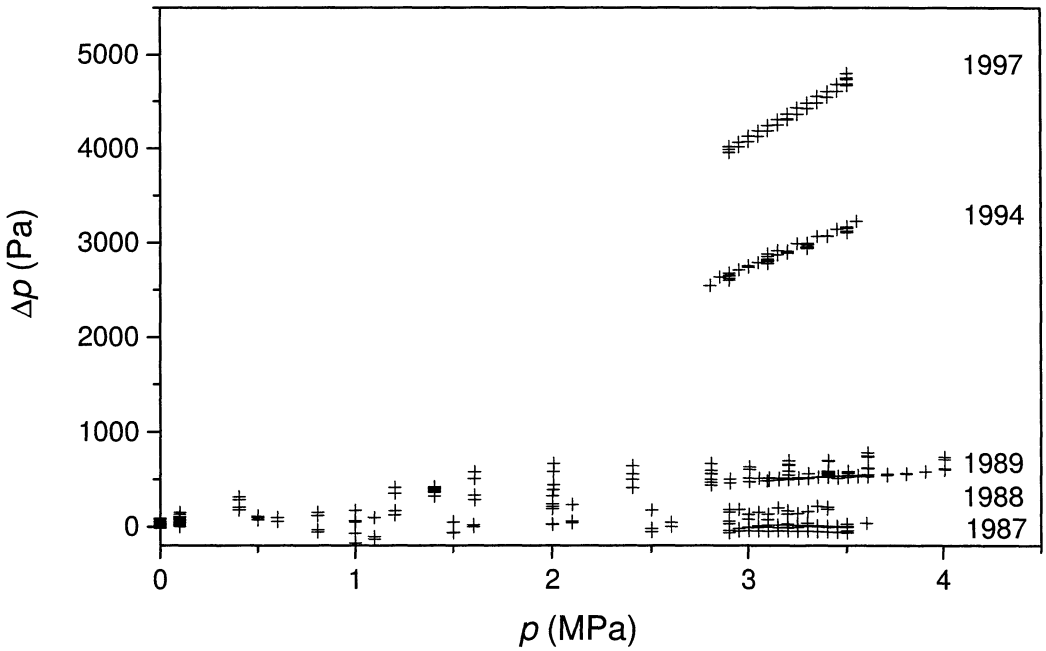

Figure 5. Variation of the slope of the pressure transducer calibration over a period of ten years. All pressure values were calculated with reference to the calibration made in 1987.

Three of these calibrations were made in the PTB pressure laboratory, all others using the pressure balance #3428. A permanent drift of the slope is clearly visible. Hence, in satisfactory approximation, the residual pressure differences are proportional to pressure, and linear fitting polynomials are sufficient for the conversion between different transducer calibrations. The latest correction is 2.3 kPa at 2.9 MPa, and 2.7 kPa at 3.5 MPa.

The instability of a newer model of the transducer (Digiquartz type 31K-101) in use at MK1 is shown in figure 6. It exhibits apparently random scatter instead of a continuous drift.

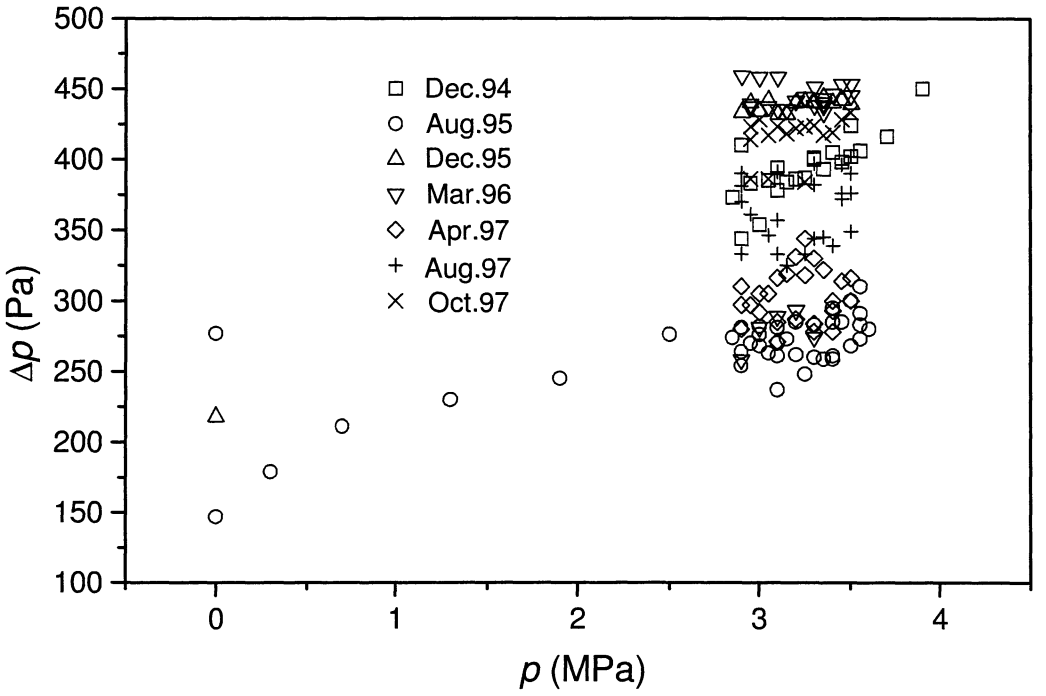

Figure 6. Calibration changes of pressure transducer type 31K-101. Pressure values of the transducer are derived from the manufacturer calibration.

The pressure transducer is situated on top the refrigerator inside a shielded room whereas the pressure balance remains outside. They are connected only during the calibration period to simplify the leak test. Clean nitrogen gas is used as a pressure medium for the calibration. In order not to contaminate the melting pressure sensor, the valve in its connection line is closed, and the calibration is made only before or after a measuring run when the melting pressure sensor is at room temperature.

The pressure balance is placed in an evacuated container, which must be pressurised before changing the mass set. Subsequently, the pressure is reduced to below 1 Pa within 5 minutes, and the set of weights is raised until it floats between the end stops by regulating the nitrogen pressure. The rotation of the piston is started, and its position is controlled manually on a constant value by adjusting the gas volume. The piston height is measured using a capacitance gauge with better than 0.1 mm resolution. Each pressure is stabilised until the measurement value becomes constant. To identify any hysteretic behaviour, the stationary pressure levels are arranged in regular intervals with growing and falling values.

A typical calibration of the pressure transducer against the pressure balance is shown in figure 7. The data points were measured over a 9 h period of time. They represent the deviation from a linear fit with a scatter of the order of 10 Pa.

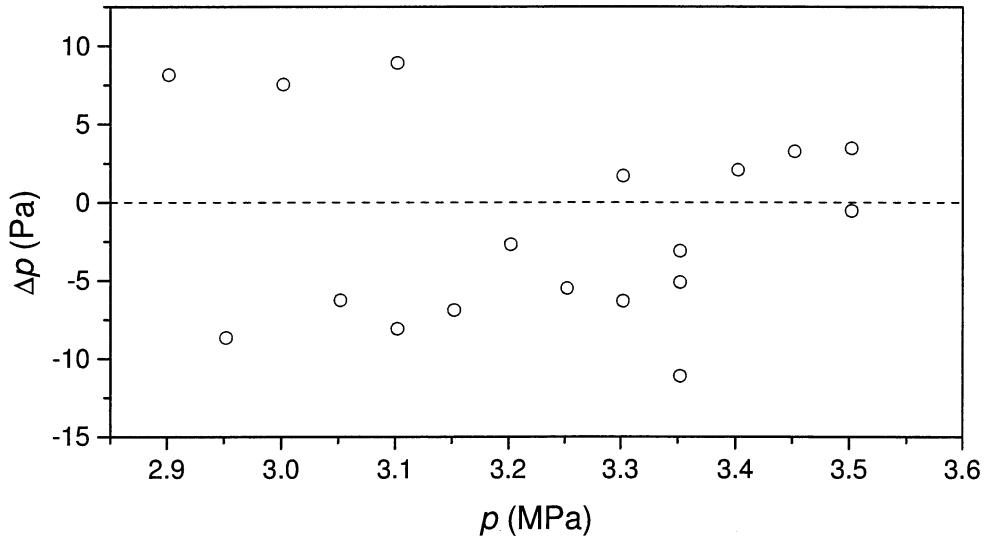

Figure 7. Pressure balance to pressure transducer calibration. Pressure deviation is taken from the linear calibration fit. Pressure transducer values are derived from the manufacturer calibration.

Calibration of the melting pressure sensor

The calibration of the ^{3}He melting pressure sensor in MK1 is always made after cooling the refrigerator to a temperature below 1.5 K. The temperature must be high enough so that no plug of solid ^{3}He appears in the capillary within the pressure range between 2.9 MPa and 4.0 MPa. Thermally caused pressure fluctuations in the experimental set-up are unavoidable due to the great lengths of the connection lines between the sensor and the pressure balance or the pressure transducer. The stabilisation of the pressure is achieved automatically if calibrations are made directly with the pressure balance where the altitude level of the piston is controlled. This is required anyway to maintain a stable effective area value. The pressure transducer is installed near to the cryostat head to keep the length of the connection tubes to the ^{3}He pressure sensor short. However, a pressure stabilisation is required in this set-up as well.

For this purpose, a buffer of approximately 0.5 cm^3 volume with a thermal link to the ^4He bath is equipped with a heater in the capillary to the sensor as described elsewhere [9]. The heater current is controlled automatically by the pressure, resulting in a pressure stability of ±2 Pa on the calibration steps of at least 1 h duration. Thus time constant effects can be identified after changes of the pressure values to preserve the precision of the final calibration.

During calibration, a capillary of 0.1 mm diameter connects the melting pressure sensor to the respective reference standard with its associated ^3He column. When the melting pressure sensor is used for temperature measurement, the connection is interrupted by solid ^3He plugs so that the weight of the ^3He gas or liquid column does not exert its pressure any more upon the sensor diaphragm. This change in operating conditions requires the application of a hydrostatic head correction. Its amount can be calculated, if the column heights and the temperatures of the pressure medium at the time of the calibration are determined.

The relevant dimensions for one of our two refrigerators are illustrated in figure 8. They comprise the heights above ground of the pressure transducer (DQ) h_{DQ}, of the 4.2 K liquid ^4He level $h_{4.2}$, of the dilution refrigerator cold plate (CP) at 1.5 K $h_{1.5}$, of the melting pressure sensor diaphragm h_{MCT}, located at the mixing chamber (MC) of the refrigerator, and of the defining area of the pressure balance h_{PrB}.

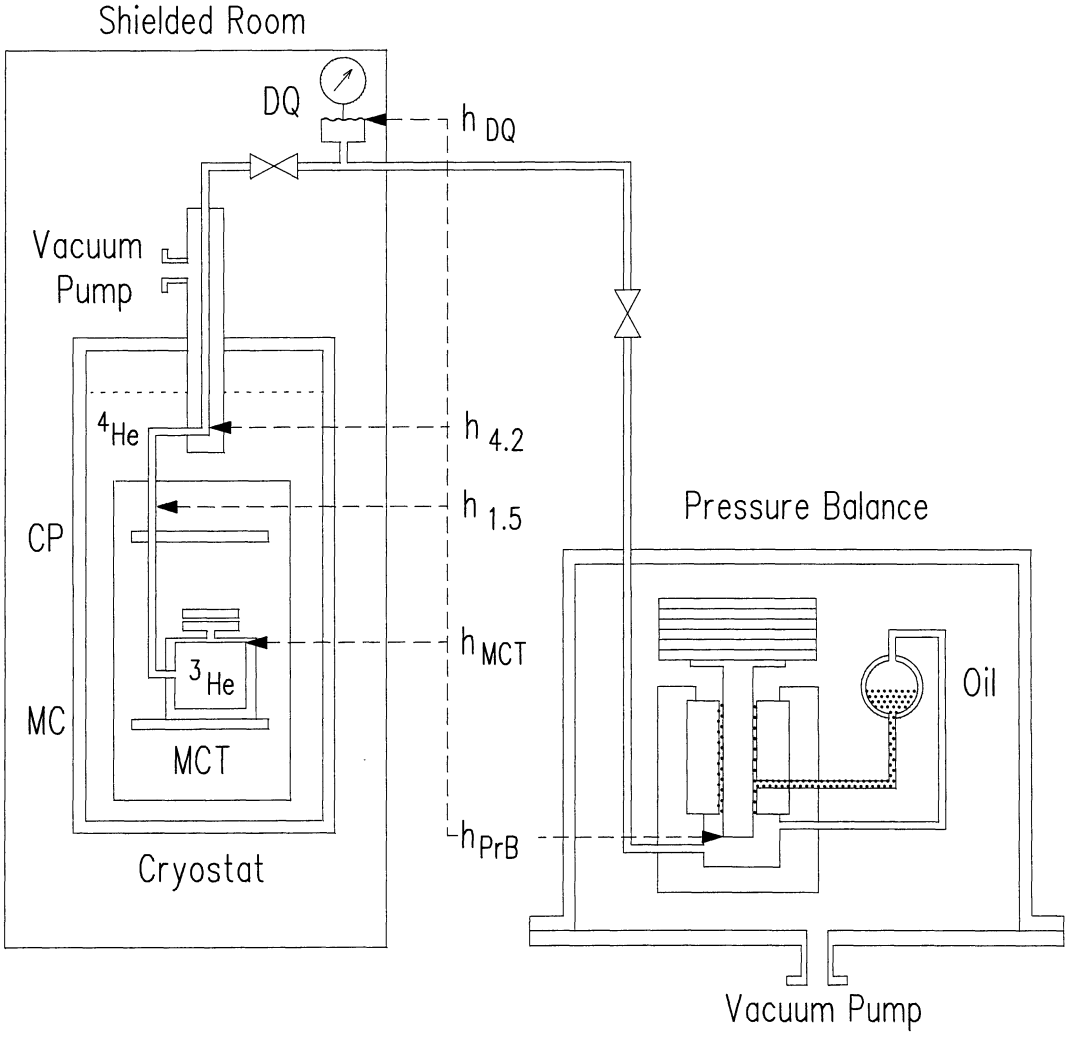

Figure 8. Rough sketch of the arrangement of melting pressure sensor in the refrigerator MK1, the pressure transducer, and the pressure balance with the valves necessary for the different calibrating possibilities.

Three regions have to be distinguished: the gas room at ambient temperature, and those of the liquid columns below 4.2 K and below 1.5 K. The densities depend on temperature and pressure. Actual values are taken from [25]. For the conditions outlined in figure 8, the values are shown in table 2 at two pressures.

Table 2. Head correction (hc) for refrigerator MK1 with ^{3}He. The calibrations are made with the pressure balance placed below the pressure sensor and with the pressure transducer placed above the melting pressure sensor.

Pressure balance						Pressure transducer		
		p = 2.9 MPa		p = 3.5 MPa			2.9 MPa	3.5 MPa
T (K)	Δh (m)	ρ (kg/m^3)	hc(Pa)	ρ (kg/m^3)	hc(Pa)	Δh (m)	hc(Pa)	hc(Pa)
298	1.213	3.58	-43	4.32	-51	0.342	12	15
4.2	0.185	111.1	202	115.4	209	0.185	202	209
1.5	0.409	115.7	464	119.4	479	0.409	464	479
Total hc			**623**		**637**		**678**	**703**

The complete vertical section extending from room temperature into the liquid ^{4}He bath is kept at 300 K by active heating. Thus the head correction depends on the horizontal transition of the ^{3}He filling-capillary from 300 K to 4.2 K with an uncertainty of ±0.5 mm. The transition from the 4.2 K area to the temperature area of the cold plate at 1.5 K is insignificant. If the transition were shifted by 1 cm, the head correction would change by only 0.5 Pa.

The altitudes were measured with a ±2 mm uncertainty in the distances inside the cryostat (according to ±2 Pa) by levelling. The transfer of the diaphragm height of the ^{3}He melting pressure sensor to the reference height of the pressure balance is uncertain by less than ±3 mm. The pressure balance is located outside the shielded room containing the cryostat. Additional dimensional uncertainties are caused by cooling down the cryostat and by uncontrolled room temperature variations. The total uncertainty, however, remains within ±5 Pa.

During sensor calibration, the pressure range was divided into two sections, a reduced range from 2.9 MPa to 3.5 MPa and an extended range from 2.9 MPa to 4 MPa, to diminish the measurement uncertainty due to sensor nonlinearity and hysteresis. Limitation to a smaller pressure range improves the pressure response of the sensor as illustrated in figure 9. The reduced range is sufficient to cover all melting temperatures below 760 mK, and calibrations in the extended range up to 4 MPa are only necessary for measurements in the temperature range 760 mK to 1 K.

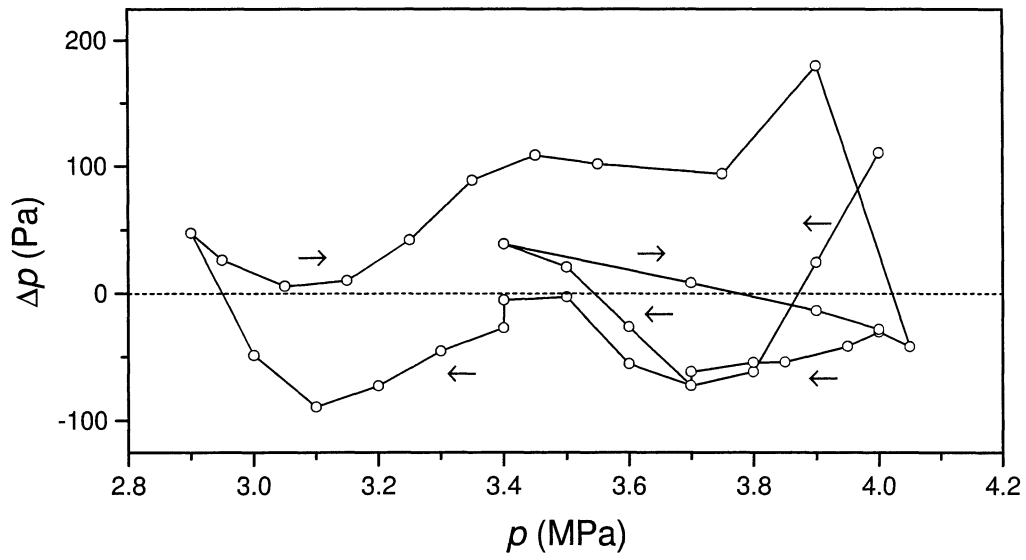

Figure 9. Melting pressure sensor calibration with the pressure transducer. Shown is the deviation of the measuring points from a third order fit which is necessary because of the extended calibration range. The temporal sequence of the measurement points is marked by a connecting line and arrows to make the hysteresis clear.

To detect any possible error sources hidden in the calibration process, also direct calibrations of the sensor were made with the pressure balance in the refrigerator MK1. In this procedure, the intermediate step using the pressure transducer was left out, and the ^{3}He filling at the room temperature end of the pressure sensor capillary reached immediately to the oil lubrication of the piston-cylinder assembly. The pressure balance itself stabilised the pressure thus avoiding also the pressure control by heating the additional ^{3}He volume in the filling capillary. Discrepancies between the two ways of operation were not observed, see figure 10.

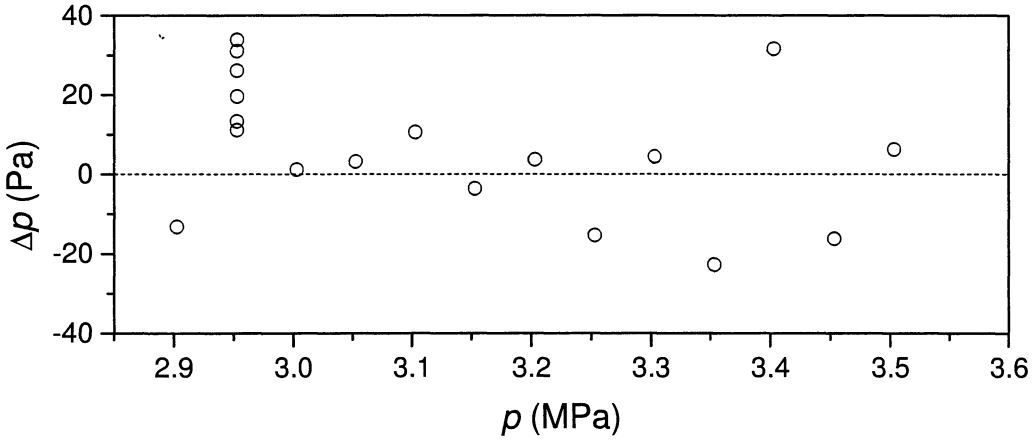

Figure 10. Direct calibration of the melting pressure sensor, made during the same measuring run as in figure 7, with ^{3}He as a pressure transfer medium. Shown are the deviations of the measurements points from a square-law fit. The points at 2.95 MPa were taken on cooling from 1.5 to 0.4 K.

Of the two differently equipped refrigerators, only MK1 had the installation to make the head correction calculable, but it did not reach temperatures range far below 10 mK. The second refrigerator, MK2 with the nuclear demagnetisation stage, was used to reach temperatures below 1 mK. The temperature range 10 mK to 1 K could be measured with both refrigerators,

which made it possible to compare different melting pressure sensors and measurement set-ups.

In the refrigerator MK2, the ^{3}He capillary runs only in a vacuum tube without temperature control straight on to the vacuum container where the melting pressure sensor is located. Consequently, the head correction depends on the temperature distribution along the capillary that is uncertain and variable with the ^{4}He level in the cryostat. Thus the estimated head correction is unreliable by up to 200 Pa. The head correction determined in the refrigerator MK1, however, made it possible to relate the data obtained during calibration and during melting pressure measurements by assigning a pressure value to the melting-pressure minimum. With this reference pressure it becomes possible to quantify the hydrostatic head itself, and calculate the its pressure-dependent corrections for the complete range between 2.9 MPa and 4 MPa. Hence, in practice, the head correction needs no longer any separate determination. It must be emphasised, however, that the precondition for this procedure is a constant hydrostatic head during the calibration without any further unidentified offsets. These could lead to large errors when extrapolating from the pressure at the minimum near to 2.9 MPa to that of the ^{3}He phase transitions near to 3.4 MPa.

Uncertainty compilation

The principal error sources of the calibrations with respect to the absolute pressure scale have already been discussed. In the following, the remaining uncertainties of the pressure balance are summarised, including those that are apparent only in the additional spread of the measurement points. These are caused, for example, by effects on the piston-cylinder unit when dismantling and reassembling the unit, by mechanical instabilities of the sensor and its pressure dependence, and by long-time drifts of the properties of the pressure balance and the sensor.

The pressure balance, used for calibration, is operated in vacuum and thus defines absolute pressure. Corrections of the air buoyancy of the mass pieces and of the air pressure are not required. Especially the independence of air pressure fluctuations favours the long-time measurements. The correct pressure values of the pressure balance are calculated from the expression:

$$p = \frac{g\sum_i m_i + 2\pi r_0\sigma}{A_0[1+2\alpha(t-20°\mathrm{C})](1+\lambda p)} + g\rho\Delta h$$

α thermal expansivity of the piston and cylinder material,
t room temperature (normally 23°C),
λ distortion coefficient of the tungsten carbide piston-cylinder unit,
ρ density of the pressure transmitting gas (N_2 or ^{3}He) with column height Δh,
σ surface tension of the lubricating oil film at the bottom of the piston-cylinder unit,
r_0 mean radius of oil film between piston and cylinder,
m_i masses of load weights.

The pressure uncertainty is determined from the root of the sum of squares of the individual contributions shown in table 3.

Table 3. Contributions of the input quantities to the pressure uncertainty of the pressure balance for three calibration pressures. If not specified explicitly, the unit of each numerical quantity is Pa. The symbol $u(x)$ denotes the uncertainty of the quantity x. The first column indicates the products of the individual uncertainties with the sensitivity coefficients. The last row is the root of the sum of squares of the individual contributions. Values in brackets denote direct calibrations obtained without the pressure transducer intermediate step and using ^{3}He instead of the otherwise employed nitrogen gas.

Pressure uncertainty at	p = 2.9 MPa	p = 3.5 MPa	p = 4.0 MPa
$p\,u(g)/g$	0.9	1.1	1.2
$p\,\sum u(m_i)/m_i$	1.3	1.3	1.3
$p\,u(A_0)/A_0$	20.7	25	28.6
$p\,2(t\text{-}20°\text{C})\,u(\alpha)$	17.4	21	24
$p\,2\alpha\,u(t)$	5.2	6.3	7.2
$p\,2\,u(\lambda)$	8.4	12.3	16
$2\pi r_0/A\;\;u(\sigma)$	0.7	0.7	0.7
$g\Delta h\,u(\rho)$	9.4 (1.2)	9.4 (1.2)	9.4 (1.2)
$g\rho\,u(\Delta h)$	3.3 (0.4)	3.9 (0.4)	4.5 (0.4)
$u(p)$	**30.5**	**36.9**	**42.6**

Additional uncertainties during sensor calibration are listed in table 4. The uncertainty of the head correction is caused by the height determination and by the density due to fluctuation of the room temperature. The pressure regulation during a calibrating value causes further uncertainties if the sensor is calibrated with the secondary pressure standard. Indicated in table 4 is the scatter of the pressure mean value generally consisting of 15 measurements averaged over one minute. The piston cylinder unit is oil lubricated. Therefore an oil drop can form at the lower piston area whose weight (approximately 50 mg) must be added to the total mass load. Another contribution follows from the different temperatures at the calibration (1.5 K) and the ^{3}He melting pressure measurement down to 1 mK because the adhesive used for the construction of the sensor has a temperature dependent dielectric constant [9, figure 20]. Its effect is indicated in the table together with the consequences of slight mechanical movements in the sensor construction observed at the melting pressure minimum.

Table 4. Uncertainty contributions to the melting pressure sensor calibration using the values from table 3. If not specified otherwise, numerical quantities are given in Pa.

Pressure	2.9 MPa	3.5 MPa	4.0 MPa
Pressure balance, table 3	31	37	43
Head correction	10	10	10
Pressure regulation	2	2	2
50 mg mass of oil drop	5	5	5
Dielectric effect	20	25	30
Total uncertainty	**38.6**	**46.1**	**53.6**

When making melting pressure measurements, the scatter of data points often is appreciably larger (e. g. Δp = 65 Pa as visible in figure 9). The main reason is mechanical hysteresis that arises in the strained components of the pressure sensor. The magnitude of the effect depends on the previous pressure values. At the limits of the calibration range it becomes small

and can assume any value in the pressure range lying between these limits up to the maximum values as illustrated in figure 11 if the pressure history is chosen appropriately.

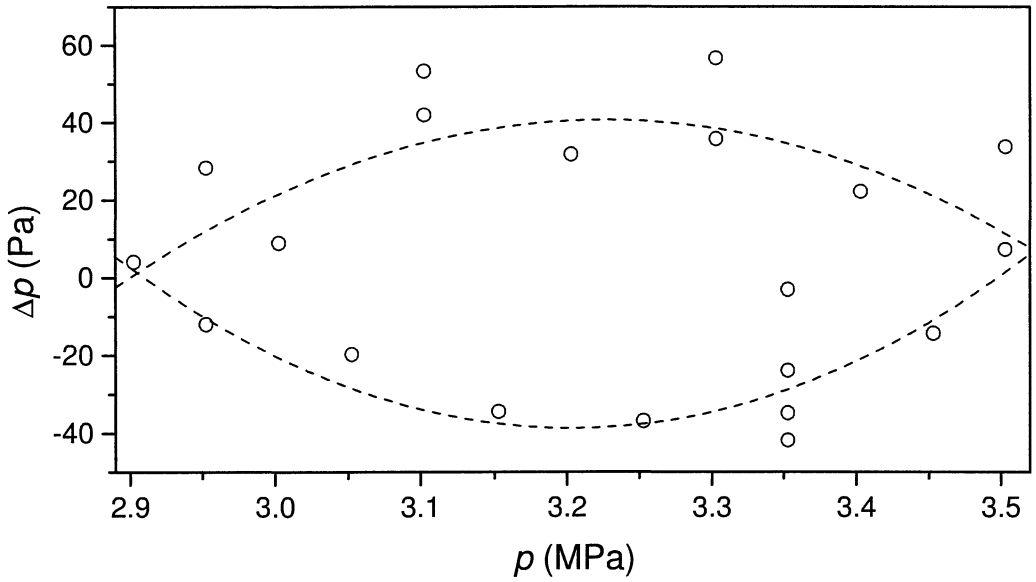

Figure 11. Deviation from linearity showing hysteresis effect between increasing and decreasing during sensor calibration with the pressure balance and ^{3}He as pressure medium in the refrigerator MK1.

The effect on the uncertainty of the pressure values can be reduced by skilful experimental tracking, for example by temperature values which are arranged with increasing and decreasing steps and by taking the mean of both directions. The uncertainty is only small at the pressures of the ^{3}He phase transitions. If the hysteresis is covered only incompletely, an additional item must be included in the uncertainty budget as indicated in table 5.

Although the melting pressure sensor is brought to a mechanically stable state by repeated load changes before a calibration, slight movements in the mechanical construction may occur during the very long measuring periods of several months at low temperature. The consequences are taken into account by assigning a non-zero uncertainty of the hysteresis effect at the lower and upper pressure limit of the calibration ranges in table 5. Larger jumps, and the effects of an accumulated drift, can be identified at the melting pressure minimum or the ^{3}He phase transitions, and a pressure correction can then be included into the calibration as a first order approximation.

Table 5. Total uncertainty of the pressure measurement including hysteresis for narrow and extended calibration ranges. If not specified otherwise, numerical quantities are given in Pa.

Calibration range	2.9 to 3.5 MPa			2.9 to 4.0 MPa		
Pressure	2.9 MPa	3.2 MPa	3.5 MPa	2.9 MPa	3.45 MPa	4.0 MPa
Uncertainty, table 4	39	43	46	39	47	54
Hysteresis effect	5	20	10	5	30	10
Total uncertainty	**40**	**48**	**47**	**40**	**56**	**55**

4. Confidence checks of PTB-96

Since PTB-96 below 40 mK has been established on the basis of a single measurement between 1 mK and 5 mK, it is prudent to check its reliability. The NMR thermometer [11] was used to confirm various temperature ratios between 115 mK and 0.88 mK. Application above 45 mK required the construction of a special sample to attain sufficient resolution. Also, to eliminate the temperature dependence of the shape of the free induction decay, only its initial amplitude obtained by back-extrapolation to the origin was employed, and a careful elimination of the temperature independent background was made. These steps were all necessary to ensure the validity of the Curie law. The measurements below 45 mK (squares in figure 12) gave a statistically insignificant systematic deviation of the melting temperature of (-0.2 ±0.2)% at 15 mK compared to that at 45 mK.

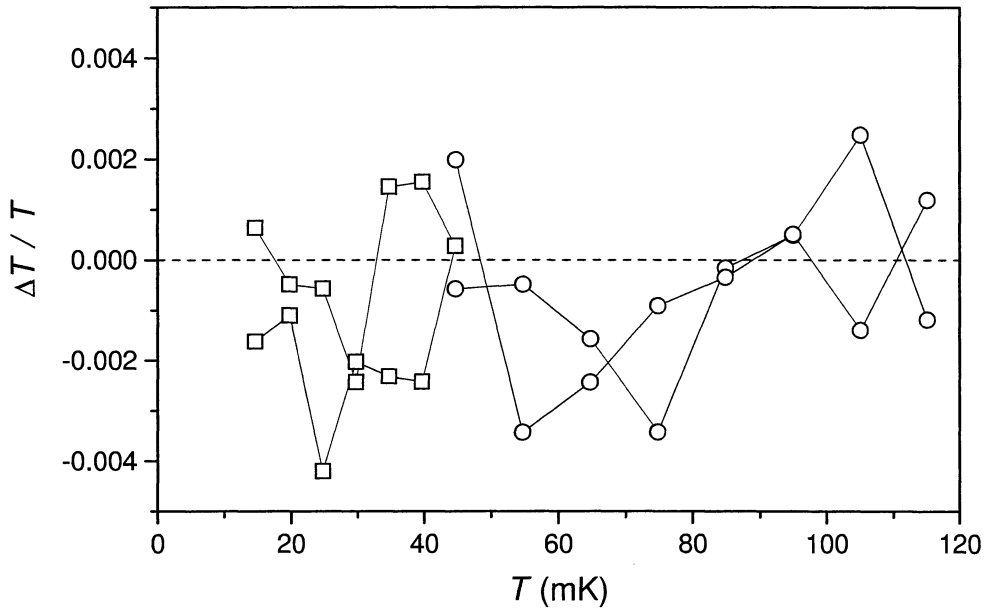

Figure 12. Relative deviation of melting temperatures from those indicated by NMR.

From observations made with a platinum sample of medium purity between 500 mK and 10 mK [26], it cannot be excluded that the back-extrapolation would compensate only for about 80% of the apparent decline of the Curie constant due to the decrease of the signal decay time with temperature. Transferring the result to the samples of high purity used here would mean that temperature ratios between 15 mK and 45 mK could be high by about 0.5%, whereas ratios between 1 mK and 15 mK could be high by 0.2%. To remove this uncertainty, the NMR results have to be checked against another thermometer, which had to be done anyway by means of noise thermometry.

Measurements between 115 mK and 45 mK (circles in figure 12) gave similar results with barely significant deviations of (–0.2 ±0.2)% near 70 mK. Thus the melting pressure equation is practically consistent with the NMR above 15 mK.

The next check using the NMR thermometer was made below 15 mK down to 2 mK. For this purpose, the Curie constant was determined at each melting temperature, and the averaged Curie constant was used to convert NMR signal amplitudes to temperatures. The result, shown in figure 13 for seven independent runs, demonstrates that the general agreement is within ±0.5%, and that the melting temperatures near 2 mK may have a systematic deviation of (+0.2 ±0.3)% compared to those at 15 mK. The temperature variation was restricted to roughly a factor of eight to obtain optimum signal parameters at the high temperature end.

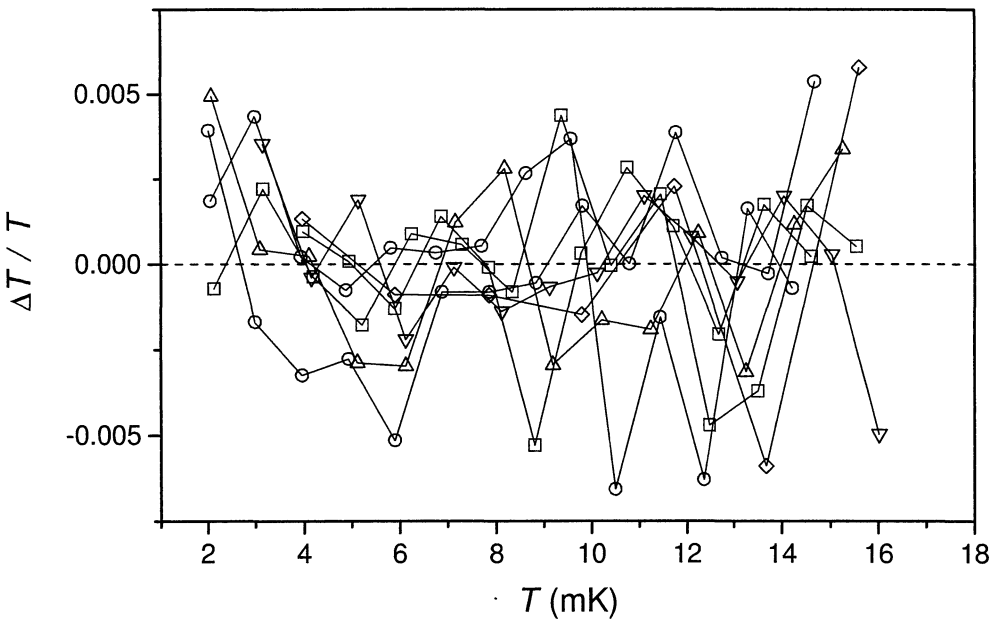

Figure 13. Relative deviation of melting temperatures from those indicated by NMR.

Deviations in the range below 3 mK are shown in figure 14. The solid data points result from direct ratio measurements made over a time interval of 20 hours sequentially at 0.9 mK, 2.7 mK and 1.1 mK. The open squares and circles represent data from two experiments that each were collected on individual temperature steps arranged with growing and falling temperatures over a time interval of 140 hours. Calibration of the NMR thermometer was made with the Curie constant determined at 2.7 mK for the ratio measurements, and with the averaged Curie constant between 1.25 mK and 2.5 mK for the step patterns. The deviations of (0.3 ±0.3)% visible at 0.9 mK are again hardly significant. Thus also below 15 mK the melting pressure equation is fully consistent with the NMR. In other words, the scale PTB-96 can replace the NMR during measurements or in the interpretation of discrepancies with other thermometers.

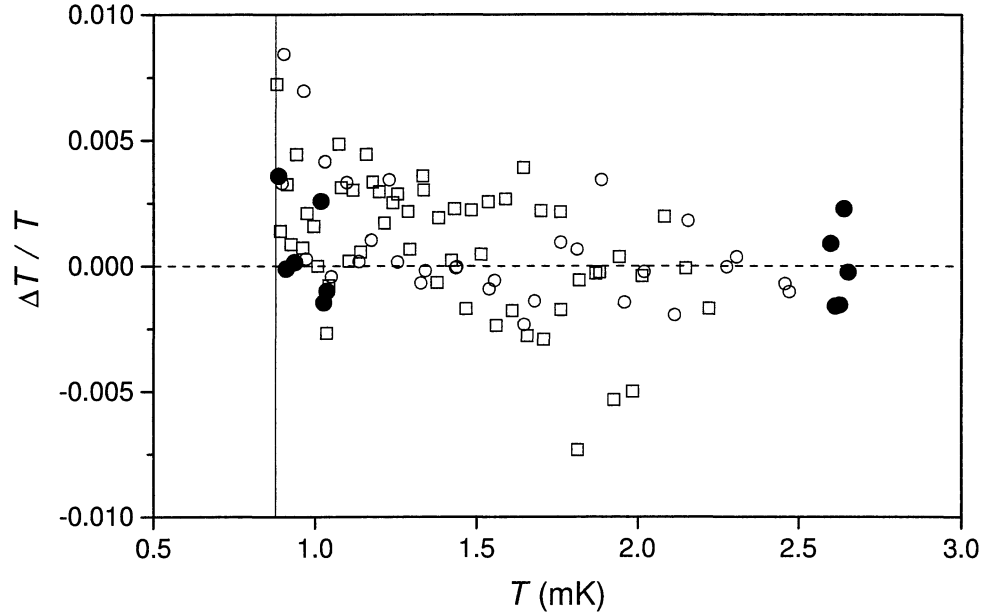

Figure 14. Relative deviation of melting temperatures from those indicated by NMR. Vertical line at 0.88 mK denotes solid ^{3}He phase transition.

5. Verification of PTB-96 with noise thermometry

The quantity measured with a noise thermometer [27] is the variance $\langle u^2 \rangle$ of voltage fluctuations which ideally are only of thermal origin and follow the familiar relation $4k\theta R\Delta f$, where k is the Boltzmann constant, θ the thermodynamic temperature, R the resistance, and Δf the bandwidth of the detector. In practice, however, it may be affected by parasitic noise with the variance $\langle u_0^2 \rangle$ introduced by the measuring equipment. Since thermal noise and parasitic noise are statistically independent, their variances simply add such that the measured noise is

$$\langle u^2 \rangle = \langle u_0^2 \rangle + 4k\theta R\Delta f.$$

The thermodynamic significance of noise thermometry is based only on the second term, the slope of the voltage variance with temperature. Therefore, a temperature scale based on noise thermometry should only rely on this slope. The offset $\langle u_0^2 \rangle$ presents no problem, if it does not depend on temperature, because it can be subtracted from the measurement result once it has been determined by an independent method. In order to separate the slope from the offset, it is necessary to relate the values, obtained from dividing $\langle u^2 \rangle$ by $4kR\Delta f$, with temperatures from a thermometer that has no inherent offset, as the NMR thermometer, over a temperature range as wide as possible. This comparison can be made equally well with PTB-96 since its temperatures were shown to be proportional to the NMR temperatures.

The actual measurements were made with a dilution refrigerator equipped with a nuclear demagnetisation stage [28] as shown schematically in figure 15. Operation below 15 mK relied on nuclear demagnetisation, and above 15 mK, with the heat switch closed, on dilution refrigeration. The sensors are attached to the upper extension of the nuclear stage, the mounting post, on the same perimeter as the NMR, an AuEr paramagnetic susceptibility thermometer [29] useful to well below 1 mK, a carbon resistance thermometer for temperature control above 15 mK, and a highly reproducible tungsten superconductive reference [30] calibrated at 15.4 mK.

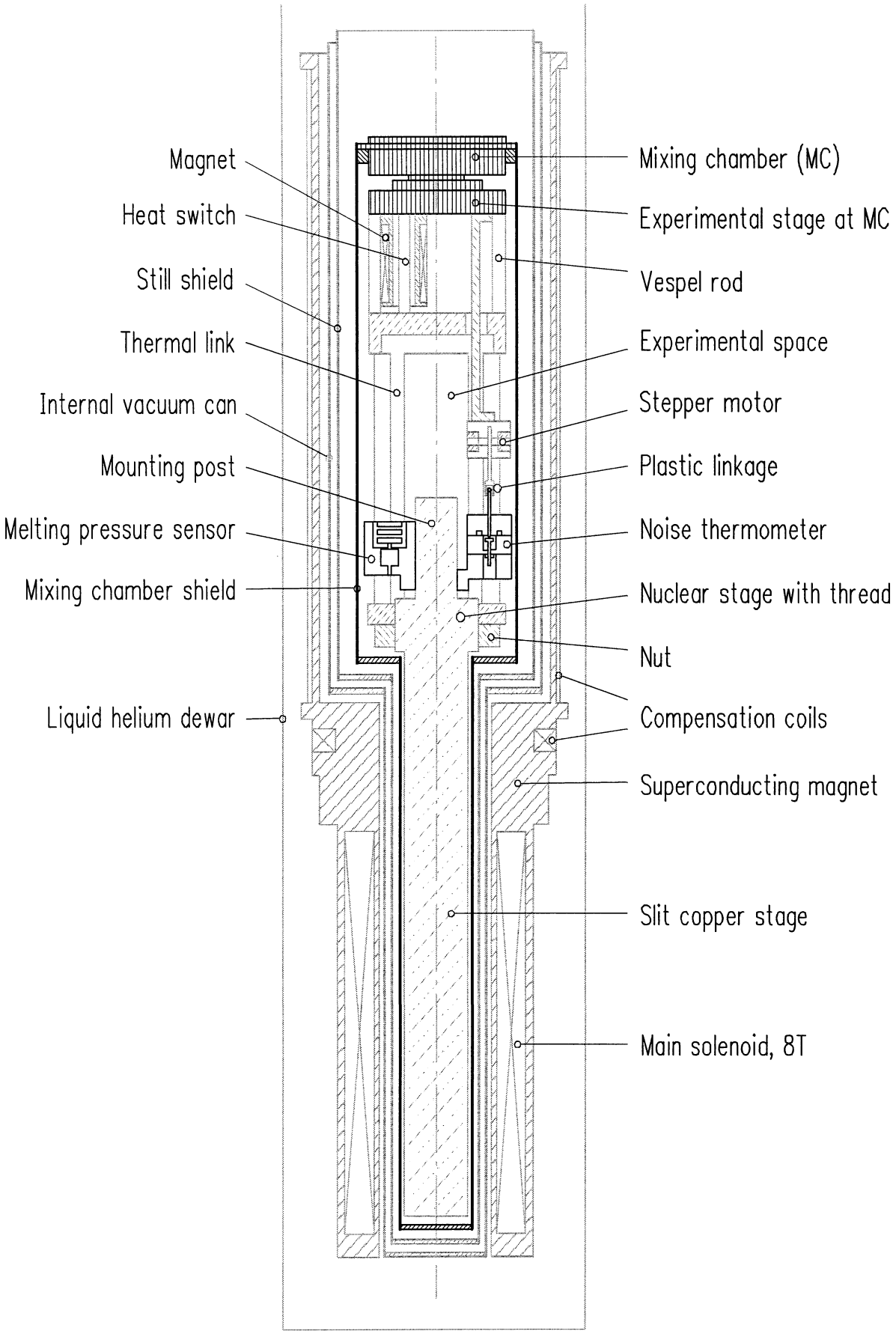

Figure 15. Mounting of thermometers on the nuclear demagnetisation stage.

The whole assembly is completely enclosed with a heat shield connected to the mixing chamber. By an independent controller, the mixing chamber temperature can be raised to above the 7 mK lower limit of the dilution refrigerator. If the heat switch is open, this feature makes it possible to change the complete parasitic heat flow from the mixing chamber to the nuclear stage. Then the non-appearance of temperature differences between the thermometers ascertains isothermal conditions. If the heat switch is closed, all temperatures up to 0.7 K can be adjusted.

Preliminary checks have shown that the main deviations between PTB-96 and the noise temperatures appear at low temperatures. They consist of a temperature independent offset and a contribution by a heat leak that causes a $1/T$ divergence. These effects need closer inspection. A different graphical representation is chosen in order to make them visible more clearly. The following diagrams represent the relative temperature differences $\Delta T/T$ as a function of the inverse temperature $1/T$. The temperature independent offset then shows up as a constant slope, the discrepancy due to the heat leak has a parabolic shape. The actual situation is shown in figure 16.

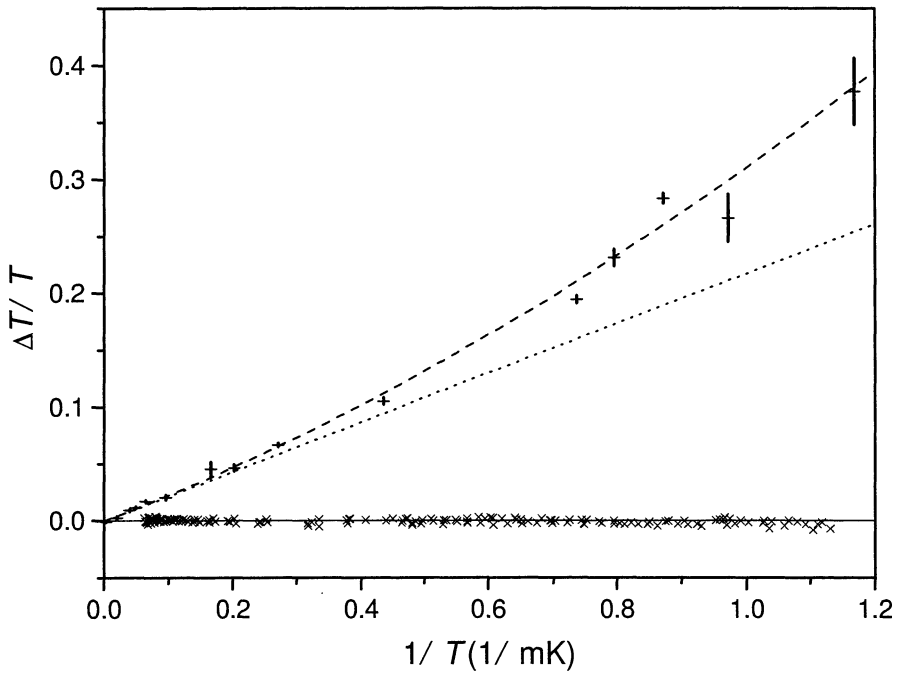

Figure 16. Relative deviations of noise (+) and NMR (×) temperatures from PTB-96. Broken line is a second order polynomial fit to the data. Dotted line is its linear component. Lengths of vertical bars denote statistical uncertainties.

As expected from the construction, the NMR temperatures agree with PTB-96. Above 5 mK, the noise temperature shows evidence of an offset of 0.22 mK, and further square-law deviations below 5 mK attributable to a heat leak. As already mentioned above, the offset is also influenced by the room temperature equipment necessary for measurement of the noise voltages. Therefore, in a new experiment, the most critical parts were placed at a temperature of 1.5 K inside the cryostat. The results are shown in figure 17. There is a clear reduction of the offset to 0.12 mK visible, although not less than with liquid nitrogen cooling. Since also the experimental conditions at very low temperatures were defined more strictly, the signature of the heat leak improved markedly so that its parabolic shape became obvious.

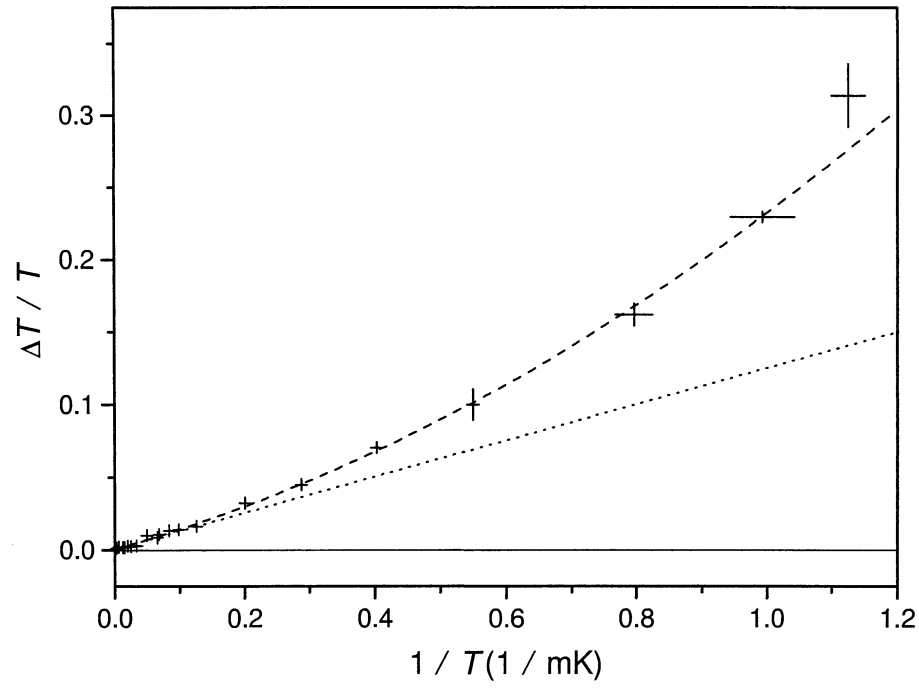

Figure 17. Relative deviations of noise (+) temperatures from PTB-96 with cooled preamplifier. Broken line is second order polynomial fit to the data, dotted line its linear component.

At least part of the offset is due to the transistor that amplifies the noise signals. Apparently, its input noise current is flowing down to the temperature sensor, and is mixed up with the thermal noise to be measured. This interpretation has been checked in a new experiment with a different type of transistor. The results are shown in figure 18.

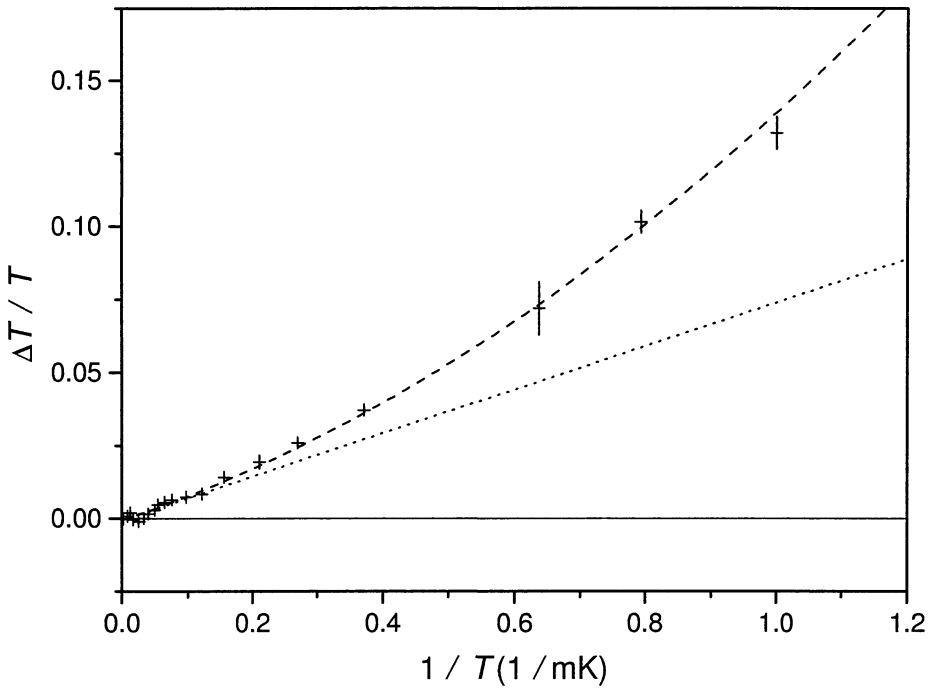

Figure 18. Relative deviations of noise temperatures (+) from PTB-96 with different type of transistor. Broken line is second order polynomial fit to the data, dotted line its linear component.

The offset decreased once more to 0.08 mK. The simultaneous drop in the heat leak, however, is not caused by the new transistor. Inspection of the heat leak had shown that it does not depend on an external source but that it is due to heat stored in the body of the noise sensor itself. This reservoir gradually releases the stored heat through the noise resistor during the measurements, and leads to a slowly decaying temperature difference. Its effect was lower in this experiment because the start of the measurements was deliberately postponed until the heat flow had fallen off significantly. In addition, accidental refilling of the heat reservoir was avoided.

With the identification of the heat source, the influence of the heat leak could be made predictable by a proper timing of the measurements, so that the effects become correctable numerically. The results of a further experiment, specially planned for this purpose, are shown in figure 19.

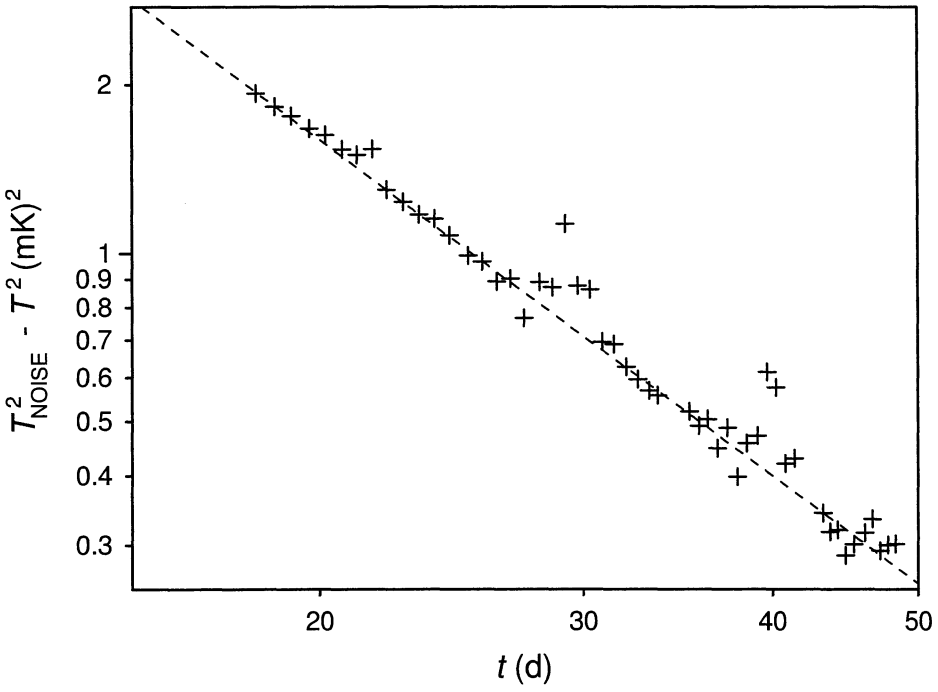

Figure 19. Decay of the heat leak. Locally varying scatter of data points is due to measurements made at different temperatures.

The variable nature of the heat leak explains also the poor reproducibility at low temperatures in figure 16. In that experiment, the scatter was a consequence of combining measurements at temperatures below 15 mK with operating periods far above 15 mK where the reservoir always received a new charge of heat.

After correction of the heat leak, figure 20 illustrates that the only remaining deviation is the temperature independent offset. Although its magnitude may perhaps be further reduced with a transistor of even lower noise current, there is no reason to expect that it can be completely removed. So the experiments with the noise thermometer were terminated at this point with the conclusion that an offset due to non-thermal noise can be corrected numerically, because it is always detectable with the platinum NMR thermometer. The necessary assumption that the offset does not originate in the NMR thermometer itself is based on the confidence that platinum NMR follows a Curie law and not a Curie-Weiss law.

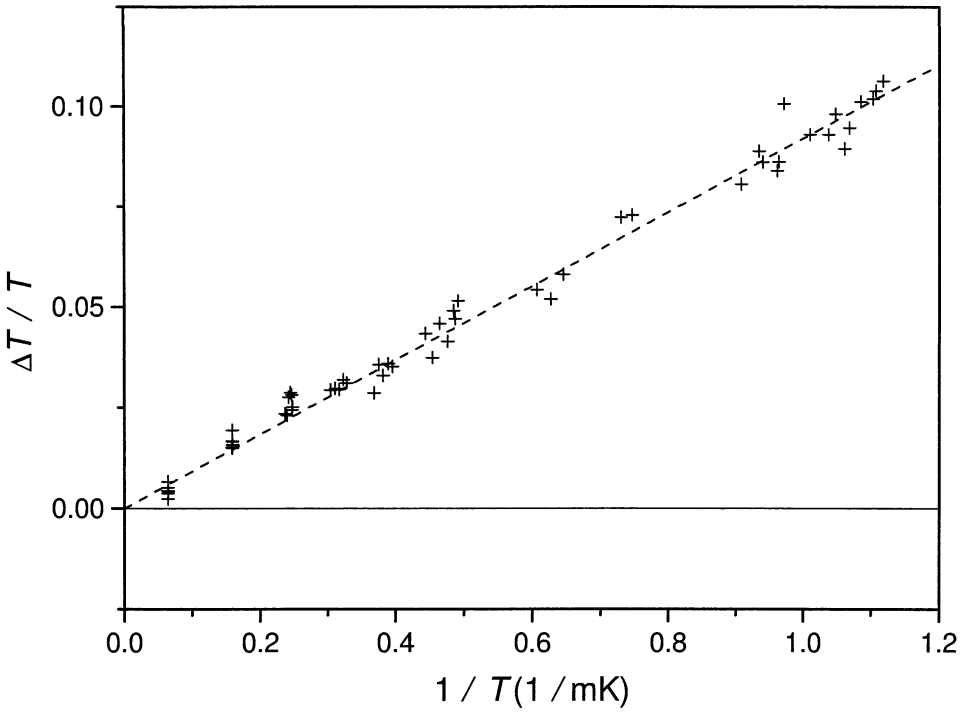

Figure 20. Relative deviations of noise temperatures (+) from PTB-96 with correction of the heat leak. Broken line is a first order polynomial fit to the data.

Since the determination of the noise offset depends on the precise realisation of the Curie law in platinum NMR, this question has been examined once more using a platinum sample made from a different material. For the results, shown in figure 21, the NMR signal amplitudes were converted to temperatures with the average Curie constant from all data.

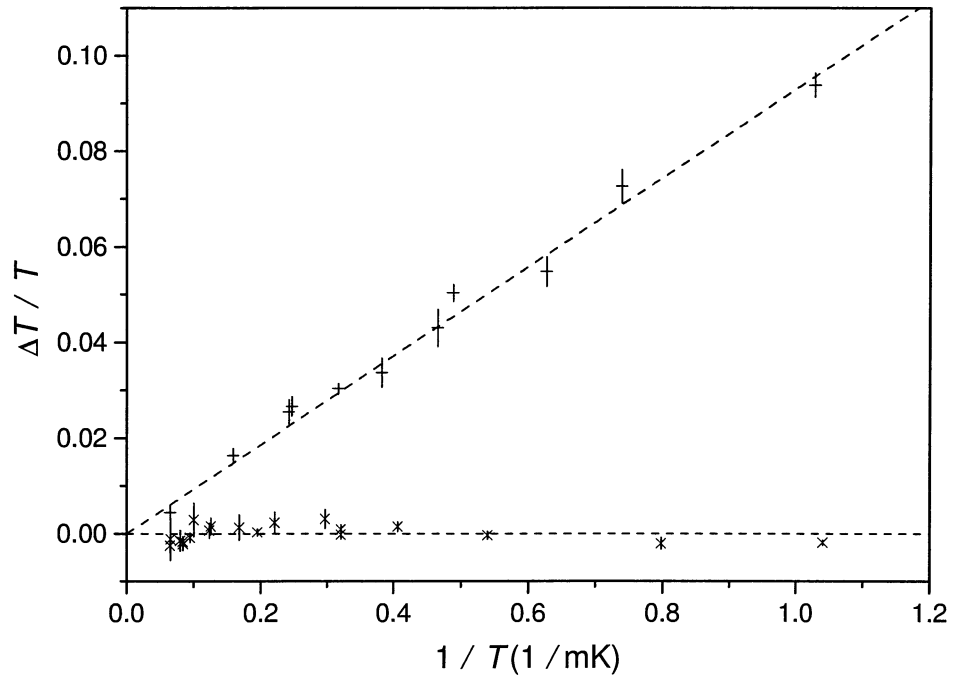

Figure 21. Relative deviations of noise (+) and NMR (×) temperatures from PTB-96. Vertical bars denote standard deviations of individual measurements. Difference of broken lines corresponds to a parasitic noise offset of 0.093 mK.

Also included in figure 21 are the noise thermometer deviations taken from figure 20, which have been collected in groups to obtain a data structure similar to that of the NMR. It can be seen that the NMR data again confirm the reference scale within ±0.3% (improving at low temperatures). The noise data are consistent with an offset of 0.093 mK, and all individual data points are located within ±0.5% of the line (improving at high temperatures). Within these uncertainty limits, it is possible to draw the following conclusions. First, PTB-96 represents the temperatures obtained by means of platinum NMR. Second, if the NMR signals follow a Curie law, the noise thermometer signals contain a temperature independent background. And third, if this offset is removed, the noise temperatures are identical with those of PTB-96. Thus, PTB-96 represents temperatures, which are as thermodynamic as those indicated by the noise thermometer.

After having made offset and heat leak corrections of the noise temperatures, a systematic difference between PTB-96 and noise temperatures appears. This can be demonstrated by making a square-law fit to the data of figures 17 and 18 of the shape

$$\frac{\Delta T}{T} = \frac{a}{T^2} + \frac{b}{T} + c$$

and calculating the residuals. The results are shown in figure 22. The diamond and square symbols denote the two experiments, which were obtained during two consecutive years with major modifications in between. In one case, the complete circuits connected to the noise sensor were kept at 1.5 K. In the other case, only the noise preamplifier was kept at 77 K and all other circuits at room temperature. The continuous curves are smooth interpolation functions of the two data sets and their average. They were included only as a guide for the eye. It can be seen that above 2 mK there are deviations of ±0.2%, reproducible within roughly ±0.05%, and that below 2 mK the statistical uncertainty is insufficient. Since there is no reason for the reproducible systematic pattern to originate in the noise thermometer, it is interpreted as nonlinearity of PTB-96 with respect to noise temperature.

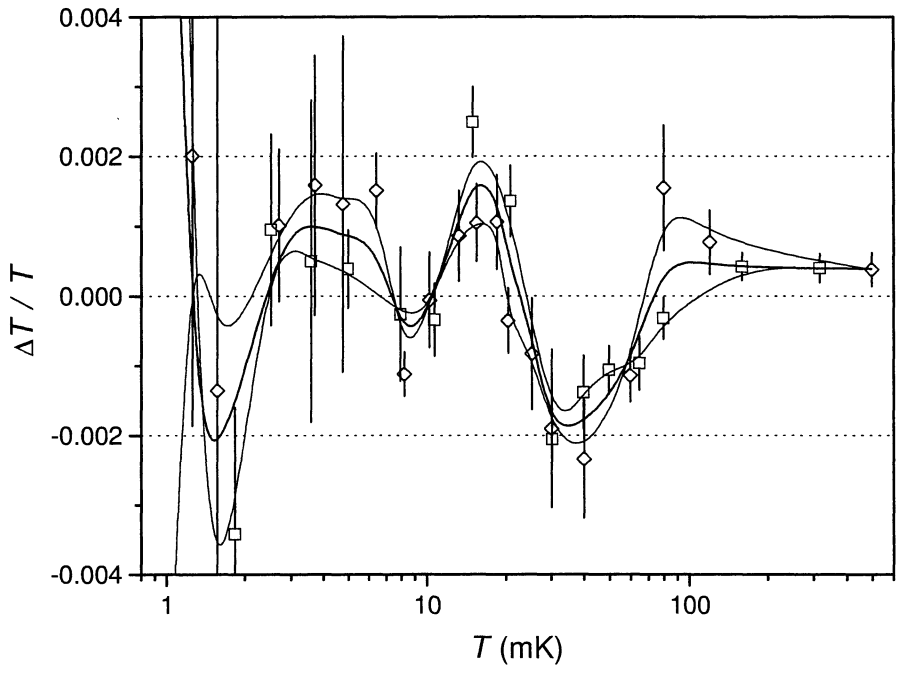

Figure 22. Deviation of corrected noise temperatures from PTB-96. Vertical bars denote statistical uncertainties.

This would be the opportunity for making a scale correction to improve its thermodynamic consistency. The actual implementation however turned out to be impracticable on the basis of the existing structure of the polynomial because neither the terms with powers in T nor those in $1/T$ are flexible enough in the temperature range between 2 mK and 100 mK to yield a better fit. Enforcing a better fit in this region only leads to unacceptable oscillations at either end of the scale. Thus the residual deviations are not caused by some mistake during the construction of PTB-96. They are rather a symptom that the shape of the polynomial describes the reality only incompletely. Since the structure of the polynomial is closely associated with the definition PTB-96 and cannot be altered, the residual variations have to be treated as additional uncertainties.

In conclusion, the model which suggests itself for PTB-96 is

$$T = T_{\mathrm{NOISE}} - T_0 - \delta/T + \Delta(T),$$

where T_0 represents the temperature independent parasitic noise voltage, δ/T the heat leak of the noise thermometer, and $\Delta(T)$ the nonlinearity of PTB-96. This means that in order to obtain the thermodynamic temperature, one has to correct the measured noise temperatures by T_0 and δ/T. The statistical uncertainty of the noise temperatures and the uncertainty of the two constants are the basis for the uncertainty estimate of PTB-96.

The background T_0 is a clear sign of temperature independent parasitic noise. A detailed investigation of its possible source revealed that it was caused by the admixture of room temperature noise to the thermal noise of the sensor resistor and not by noise simply added during signal processing [27]. Cooling parts of the electronic equipment to liquid nitrogen temperature reduced the background from roughly 0.2 mK to 0.1 mK. By changing the offset from 0.4 mK to 0.055 mK [27], it was also demonstrated that another fraction of the background depends on adjustments that can not be made perfectly reproducible. All such shifts in the background due to changing experimental conditions, however, have no influence on a temperature scale as long as it is based only on the slope of the noise voltage variances with respect to temperature.

The steep rise at the lowest temperatures is caused by a heat leak from the body of the noise resistor. Its shape depends on details of the heat conduction between the noise resistor and the isothermal surface common with the melting pressure sensor [27]. In general, such a deviation may be a complicated function of the inverse temperature. The worst case, because it is dying off so slowly towards higher temperatures, is a $1/T$ dependence, which arises if electronic heat conduction is the dominating process. This case agrees with the observation. It contributes less than 5 μK above 15 mK.

PTB-96 agrees with the noise temperatures within the linearity limits of ±0.2% if the influence of the heat leak and the offset are properly corrected. Correction of the heat leak can be made after observing the noise temperature variation with time at constant temperature. The identification of the offset requires additional input by a different thermometer. The perfect companion is the NMR thermometer because it is not affected itself by offset problems.

Noise temperature measurements above 15 mK are less affected by an offset, because it is a comparatively small quantity, but by the time required to obtain statistically significant results. The collection of all relevant data up to 500 mK gave a (0.015 ±0.065)% residual deviation of PTB-96 from the noise temperatures. A single test made at 736 mK with ± 0.2 mK uncertainty limits supports this general view. For evaluating the thermodynamic accuracy of the PTB-96 in the whole range from 0.2 K to 1 K, the noise thermometry data were used to reanalyse the CMN temperature data as carried by a RIR [31].

The total uncertainty of PTB-96 with respect to noise temperatures is a combination of the uncertainties due to heat leak and offset corrections, the statistical uncertainty of the noise

measurements, and the residual uncertainty associated with the polynomial representation discussed above. The data are collected in figure 23. The uncertainty is mainly determined by the ability to correct for the heat leak (a) and the offset (b) of the noise thermometer at the lowest temperatures [27,31]. The effect that limits the uncertainty at high temperatures is the statistical nature of the noise measurements (c). Above 0.5 K, the re-analysis of the CMN temperature data causes an additional uncertainty component [31]. At intermediate temperatures, the nonlinearity of PTB-96 (d) with respect to the noise thermometer contributes the major portion. The total estimated uncertainty (solid symbols) has been obtained as root of the sum of squares. It can be seen that the relative temperature uncertainty of the scale grows by roughly a factor of 2.5 per temperature decade from about 0.06% at 1 K to about 1% at 1 mK.

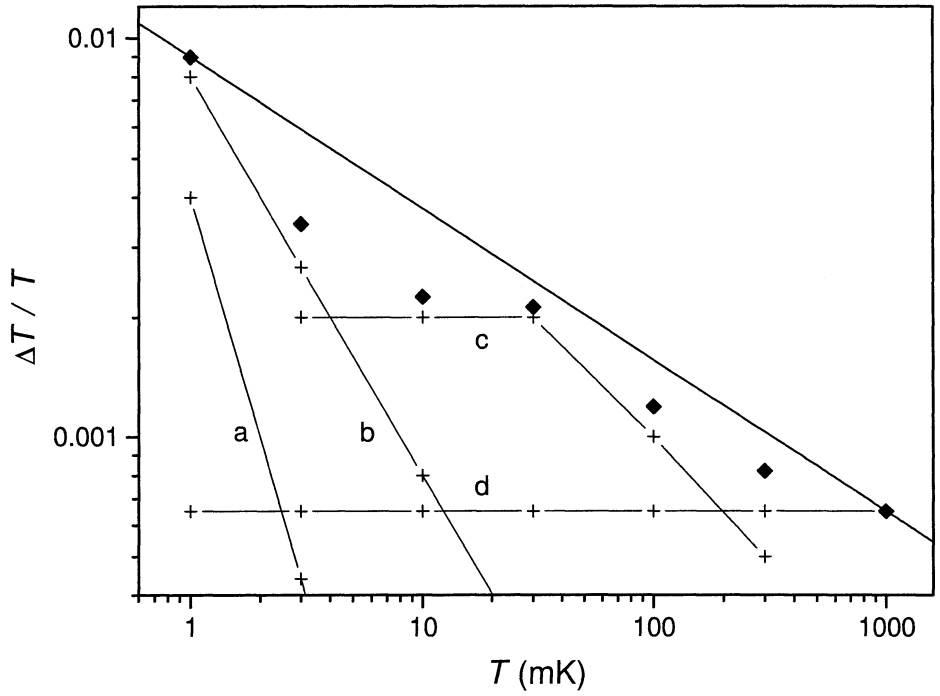

Figure 23. Relative uncertainty of PTB-96 with respect to noise temperatures (solid symbols). Crosses indicate its constituents. Continuous lines are guides for the eye to identify elements with common origin (see text).

6. Thermodynamic consistency

Since PTB-96 relies on ^{3}He melting pressure, there is an opportunity to check its thermodynamic consistency using the Clausius-Clapeyron equation that relates the entropies of liquid and solid ^{3}He to the slope of the melting pressure with respect to thermodynamic temperature. The entropies, in turn, are related to the ^{3}He specific heats.

In this chapter, a temperature scale will be developed from the specific heat values of liquid and solid ^{3}He that is thermodynamic if a number of preconditions specified below are fulfilled. The combination of specific heat measurements by Greywall [32,33] with the PTB melting pressure equation makes it then possible to characterise the thermodynamic consistency of PTB-96 or the quality of the specific heat values. T denotes the temperature of PTB-96 at melting pressure p, and θ the thermodynamic temperature at the same pressure. All quantities due to Greywall are marked by a star symbol.

Starting point is the relation between the slope of the entropy S along the melting curve and the specific heat C at melting temperature and pressure

$$C = \theta \frac{\mathrm{d}S}{\mathrm{d}\theta}, \tag{1}$$

for each solid and liquid ^{3}He. With the intention to make use of the Clausius-Clapeyron equation, the presence of both liquid and solid ^{3}He at melting is taken into account by defining the differences of molar entropies, specific heats, and volumes

$$\Delta S = S_\mathrm{L} - S_\mathrm{S}$$
$$\Delta C = C_\mathrm{L} - C_\mathrm{S}$$
$$\Delta V = V_\mathrm{L} - V_\mathrm{S}.$$

Partial integration of equation (1) with these relations results in

$$\int_{\theta_0}^{\theta} \Delta C \mathrm{d}T' = \theta \Delta S - \theta_0 (\Delta S)_{\theta_0} - \int_{\theta_0}^{\theta} \Delta S \, \mathrm{d}T'. \tag{2}$$

The Clausius-Clapeyron equation

$$\Delta S = \Delta V \frac{\mathrm{d}p}{\mathrm{d}\theta} \tag{3}$$

is applied to introduce the melting pressure. Also, due to its weak temperature dependence, the volume difference is assumed to be constant

$$\Delta V = \Delta V_0.$$

Then the rearrangement of equation (2) leads to

$$\theta \frac{\mathrm{d}p}{\mathrm{d}\theta} = \theta_0 \left(\frac{\mathrm{d}p}{\mathrm{d}\theta} \right)_{\theta_0} + \int_{\theta_0}^{\theta} \frac{\mathrm{d}p}{\mathrm{d}T'} \mathrm{d}T' + \frac{1}{\Delta V_0} \int_{\theta_0}^{\theta} \Delta C \mathrm{d}T', \tag{4}$$

which can be used to calculate θ from the melting pressure p, provided that ΔC is known. It is, however, sufficient that ΔC^* has been correctly determined using an empirical temperature scale T^* along with a melting pressure equation $p = p(T^*)$, because in this case

$$\int_{\theta_0}^{\theta} \Delta C \, \mathrm{d}T' = \int_{T^*_0}^{T^*} \Delta C^* \mathrm{d}T', \tag{5}$$

where θ and T^* are representing the same melting pressure. This equation essentially means that the heat required to change the melting pressure between two different levels is independent of the temperature scale. Substituting also

$$\frac{\mathrm{d}p}{\mathrm{d}\theta} = \frac{\mathrm{d}p}{\mathrm{d}T} \frac{\mathrm{d}T}{\mathrm{d}\theta},$$

equation (4) turns into

$$\theta\frac{\mathrm{d}T}{\mathrm{d}\theta} = \frac{\theta_0\left(\frac{\mathrm{d}T}{\mathrm{d}\theta}\right)_{\theta_0}\left(\left(\frac{\mathrm{d}p}{\mathrm{d}T}\right)_{T_0} + p(T) - p(T_0) + \frac{1}{\Delta V_0}\int_{T_0^*}^{T^*}\Delta C^*\,\mathrm{d}T'\right)}{\frac{\mathrm{d}p}{\mathrm{d}T}}, \tag{6}$$

where again θ, T and T^* represent the same melting pressure. Its general structure is

$$\theta\frac{\mathrm{d}T}{\mathrm{d}\theta} = f(T),$$

which can be integrated by separation of variables to result in

$$\theta = \theta_0 \exp\left(\int_{T_0}^{T}\frac{\mathrm{d}T'}{f(T')}\right),$$

if it is possible to assign values to the constants carrying the index 0. Particularly, the relation

$$\theta_0\left(\frac{\mathrm{d}T}{\mathrm{d}\theta}\right)_{\theta_0} = T_0, \tag{7}$$

which means that T is proportional to the thermodynamic temperature at T_0, may be helpful in this respect. If condition (7) applies, and in addition $T_0 = \theta_0$, T will be called thermodynamic at T_0.

Summarising now all preconditions, we can state: If

1) ΔC^* has been determined without any errors on the temperature scale T^* together with a ^{3}He melting pressure p^*,
2) ΔV does not depend on temperature,
3) T is thermodynamic at one specified temperature T_0,

then the thermodynamic temperature θ can be calculated everywhere else. Thus the deviation of T from θ can be determined at any temperature if T represents the thermodynamic temperature at one single specified point.

For the following discussion, it is necessary to examine these preconditions in detail. The analysis will be restricted to the temperature range below 25 mK. First of all, it is assumed that condition 1) is applicable. The numerical values of ΔC^* as a function of T^* and ΔV_0 are taken from the data collected in [34] in order to avoid ambiguities. Second, it is assumed that T^* represents the melting pressure p^* [33]. The difference between p and p^* can only be established exactly at the ^{3}He phase transitions, where pressure and temperature determinations are independent of each other. Therefore the analysis will involve the cases with reference temperatures at the solid ^{3}He transition T_N, and the ^{3}He superfluid transition T_A. In addition, the superconductive transition temperature T_W of tungsten is included because it is an important reference point for the definition of T as well as that of T^*. Further, it is assumed that the melting pressures p and p^* at the same physical temperature differ by a constant amount. This is justified because the pressure range below 25 mK is so small that nonlinearities are negligible, and the difference between additive (offset) and multiplicative (slope) deviations is insig-

nificant. Condition 2) is not regarded as serious because the temperature variation of ΔV is so weak, that it does not influence the conclusions significantly.

The result of the evaluation of equation (6) is shown in figure 24 if T is assumed to be thermodynamic at T_N, T_A, and T_W. It can be seen that PTB-96 is apparently high by 2% compared to θ at 15 mK in the first two cases. In the third case, PTB-96 is 10% high at 1 mK with a discrepancy nearly proportional to the inverse temperature, which would mean that the NMR signal follows a Curie-Weiss law below roughly 4 mK with saturation at 100 μK. In any case, PTB-96 is thermodynamically consistent with the ^{3}He specific heats either below 4 mK or above 4 mK, but exhibits a distinctive curvature near 4 mK. Since this feature does not appear in the difference between noise and NMR temperatures, it must be associated with the melting curve, either due to an imperfect realisation of the ^{3}He melting temperature or to a defect in the specific heat values.

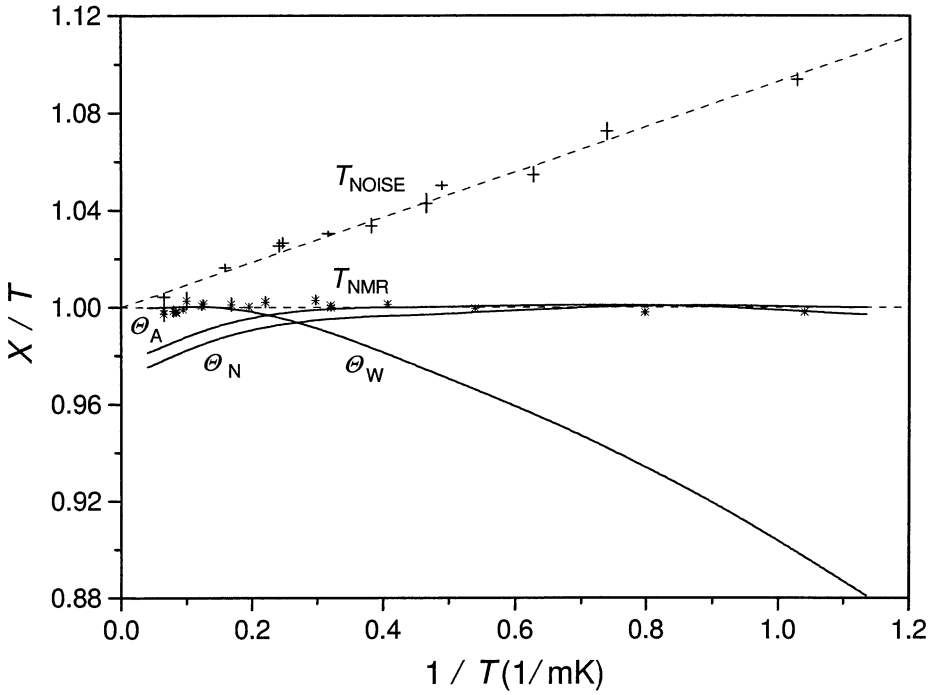

Figure 24. Temperature ratio assuming PTB-96 to be thermodynamic at the solid (N) and superfluid (A) ^{3}He phase transitions, and the superconductive transition (W) of tungsten. The experimental data of noise and NMR temperature of figure 21 are included to illustrate uncertainties. X denotes alternatively the parameter near to each curve.

One option is that the temperature of the ^{3}He filling of the melting pressure sensor does not coincide with the temperature indicated by the noise and NMR thermometers due to some kind of unidentified heat leak. An external heat leak was excluded by raising the mixing chamber temperature of the refrigerator when operated in the nuclear demagnetisation mode, which altered all indicated temperatures significantly, but had no effect on the differences. A simulated internal heat leak, by raising the sensor excitation, showed that its effect would be a parabolic curvature proportional to $1/T^2$ causing the most serious temperature divergence at the lowest temperatures, just where the specific heats confirm PTB-96.

The other option is that the discrepancy is caused by imperfections of the ^{3}He specific heat values that become relevant at temperatures above 4 mK. Specific heat measurements of a material are made by application of an infinitesimal amount of heat δQ to a sample of the material and observing its temperature rise δT. Such measurements are notoriously difficult because they require to estimate the unavoidable heat lost by conduction that has no effect on

the sample temperature. Any misjudgement in this respect may lead to systematic errors in the specific heat. Moreover, liquid and solid specific heats were measured in quite different experimental arrangements with different potential systematic error sources. In addition, the specific heat of solid ^{3}He falls with roughly $1/T^2$, and that of liquid ^{3}He grows with T. Near 7 mK both quantities are equal and ΔC disappears. Thus the temperature range below 7 mK is dominated by the solid specific heat, whereas the liquid specific prevails above 7 mK with a slope discontinuity of the difference in between.

A way to compare the essential features of specific heat measurements, which is raising the temperature by heating, with PTB-96 can be obtained from a rearrangement of equation (6). With T_N as initial temperature, it becomes

$$\int_{T^*_N}^{T^*} \Delta C^* \mathrm{d}T' = \Delta V_0 \left(\theta \frac{\mathrm{d}T}{\mathrm{d}\theta} \frac{\mathrm{d}p}{\mathrm{d}T} - \theta_N \left(\frac{\mathrm{d}T}{\mathrm{d}\theta} \right)_{\theta_N} \left(\frac{\mathrm{d}p}{\mathrm{d}T} \right)_{T_N} - p(T) + p(T_N) \right).$$

This equation permits the comparison of the heats accumulated on the way from the solid ^{3}He phase transition at T_N to any particular melting temperature T (the left hand side), with that required if PTB-96 is assumed to be thermodynamic (the right hand side), where again T^*, θ, and T are the temperatures belonging to the same melting pressure. As indicated by the difference in figure 25, the heat exceeds the requirement suggested by a Curie law of the NMR significantly, which could be caused by solid specific heat values that are too high. It is not possible, however, to go into further details with this issue because, due to the double integration on the way from the specific heats to the temperature scale, most features characterising the shape of the deviation are lost. Thus the analysis of different error models yield as result that the solid specific heat must be inaccurate by 3% to 6% depending on the actual cause

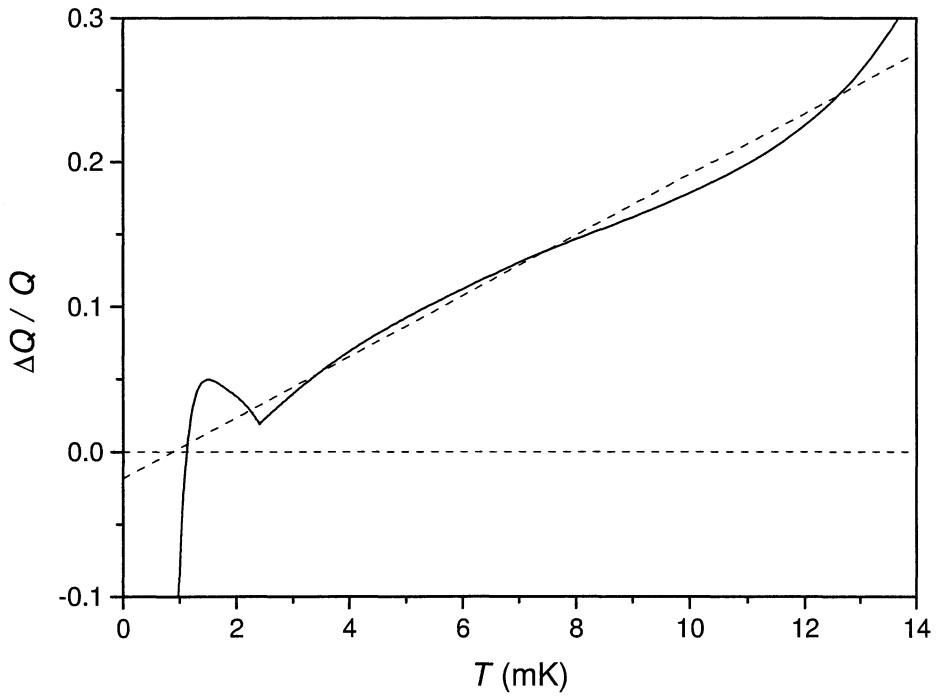

Figure 25. Relative heat difference, which has been calculated from specific heat data and from PTB-96, accumulated on the way from T_N to T.

In conclusion, there is a clear discrepancy between the temperature scale calculated from the specific heats and PTB-96. Its cause may be each, violation of the Curie law of platinum

NMR and unidentified nonlinearities of noise thermometry that cancel each other exactly, a temperature of the melting ^{3}He that does not agree with that of the thermometers, or an insufficient accuracy of the specific heat values. The source can not be definitely assigned to either alternative.

Any attempt to save the Curie law, however, requires some kind of modification of the specific heats, which may even appear quite reasonable, but remains arbitrary in the end. PTB-96 is based on the confidence that the Curie law holds down to 1 mK because no evidence on its breakdown is available. Experimental mistakes have been excluded by changing instrumentation, data processing, and sample materials with always consistent results.

7. Temperature scale comparisons

Due to its excellent reproducibility, the ^{3}He melting curve lends itself well to temperature scale comparisons without the exchange of calibrated devices or even of complete thermometers. Definite conclusions on temperature scale differences, however, can only be drawn if there is no uncertainty with respect to the pressure scales. The ^{3}He phase transitions below 2.5 mK (table 6) and the pressure minimum near 315 mK (table 7) provide the means to efficiently remove ambiguities due to pressure scales. In the temperature range below 15 mK, pressure corrections can be simply made by addition of the differences found at the solid ^{3}He phase transition. For this narrow range of approximately 60 kPa, the variations of the differences with pressure are practically negligible.

Table 6. Melting temperatures and pressures at the ^{3}He phase transitions.

	Halperin *et al.* 1978 [35]	Greywall 1986 [32]	Fukuyama *et al.* 1987 [36]	Ni *et al.* 1995 [37]	PTB-96 [2]	PLTS-2000 [1]
T_N / mK	1.10 ±0.06	0.931 ±0.008	0.914 ±0.012	0.934 ±0.009	0.88 ±0.01	0.902
T_B / mK	2.18 ±0.10	1.932 ±0.015	1.933 ±0.021	1.948 ±0.020	1.87 ±0.02	1.896
T_A / mK	2.75 ±0.11	2.491 ±0.020	2.477 ±0.026	2.505 ±0.025	2.41 ±0.02	2.444
p_N / MPa	3.43943	3.43905	3.43930	3.43899	3.43928	3.43934
p_B / MPa	3.43619	3.43580	3.43605	3.43575	3.43603	3.43609
p_A / MPa	3.43420	3.43380	3.43403	3.43376	3.43401	3.43407
Δp / Pa	±300	±300	±800	±100	±80	

Table 7. Pressures and temperatures at the melting curve minimum.

	p_{MIN}/MPa		T_{MIN}/mK
Grilly 1971 [38]	2.9315	±300 Pa	319 ±3
Halperin et al.1978 [35]	2.9316	±300 Pa	
Greywall 1985 [39]	2.93175	±300 Pa	316 ±1
Schuster et al. 1990 [40]			315.1 ±0.3
Colwell et al. 1992 [25]	2.931184	±60 Pa	
Fogle et al. 1992 [41]			315.23 ±0.09
Bremer and Durieux 1992 [42]	2.93114	±180 Pa	
PTB-96 [2]	2.93107	±50 Pa	315.17 ±0.15
PLTS-2000 [1]	2.93113		315.24

The temperature scales in this range, due to Greywall [32], Fukuyama *et al.* [36], Ni *et al.* [37], and Fogle and Soulen [43], are all available as polynomial representations of the melting pressure as a function of temperature. Whereas the scale of Fogle and Soulen relies on noise thermometry, the other scales use mainly magnetic thermometry to reach the lowest tempera-

tures from an initial temperature in the vicinity of 15 mK. Greywall chose the susceptibility of lanthanum diluted cerium magnesium nitrate (LCMN) to extend his temperature scale, constructed by means of a superconductive fixed point device from NIST, to below the tungsten transition. Fukuyama *et al.* used the Greywall results for an extrapolation with a platinum NMR thermometer. Ni *et al.* used platinum NMR in combination with a nuclear orientation thermometer below 25 mK. As shown in figure 26, the temperature differences between the scales are increasing from values of 2% or less at 15 mK to nearly 6% below 1 mK where all the scales are expected to be accurate within ±1%.

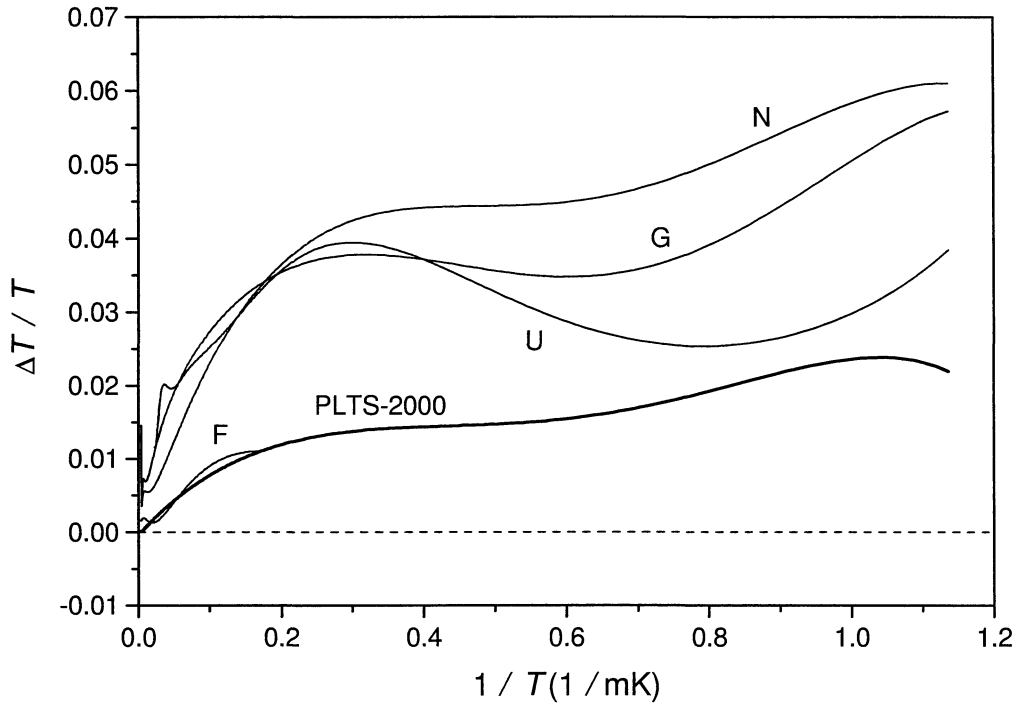

Figure 26. Relative deviations of ^{3}He melting temperatures of Greywall (G), Fukuyama *et al.* (U), Ni *et al.* (N), Fogle and Soulen (F), and PLTS-2000 from PTB-96.

The pressure corrections of the Fogle and Soulen (NIST) scale could be restricted to the differences at the melting curve minimum because the residual deviations at the tungsten superconductive transition were negligible. It can be seen from figure 27, that the relation between the NIST scale and the PTB scale is clearly linear with an offset of 70 μK and a slope of 0.1%, and deviations from linearity within ±0.1%. This linear relation has to be attributed to a discrepancy between the noise thermometers at NIST and at PTB because both scales agree with their own noise thermometry.

The offset between the NIST and PTB scales is the dominating discrepancy at low temperatures. Since some problem of this kind can always be expected with noise thermometry, the NIST scale relies on a nuclear orientation thermometry to conclude that there is no offset, whereas PTB uses NMR thermometry to correct an existing offset. Thus the discrepancy may be caused either by an unsuspected offset of the nuclear orientation thermometer of NIST or a misinterpretation of the offset of the PTB noise thermometer. This puzzle can only be solved by introducing additional information, e. g. by making a cross check between the NMR and nuclear orientation thermometers. It is not possible to use the other low temperature scales available to settle the matter, because at 6.3 mK, which is the lowest temperature of the NIST scale, decision has to be made about a quantity of 70 μK which is near to the precision limit of those scales.

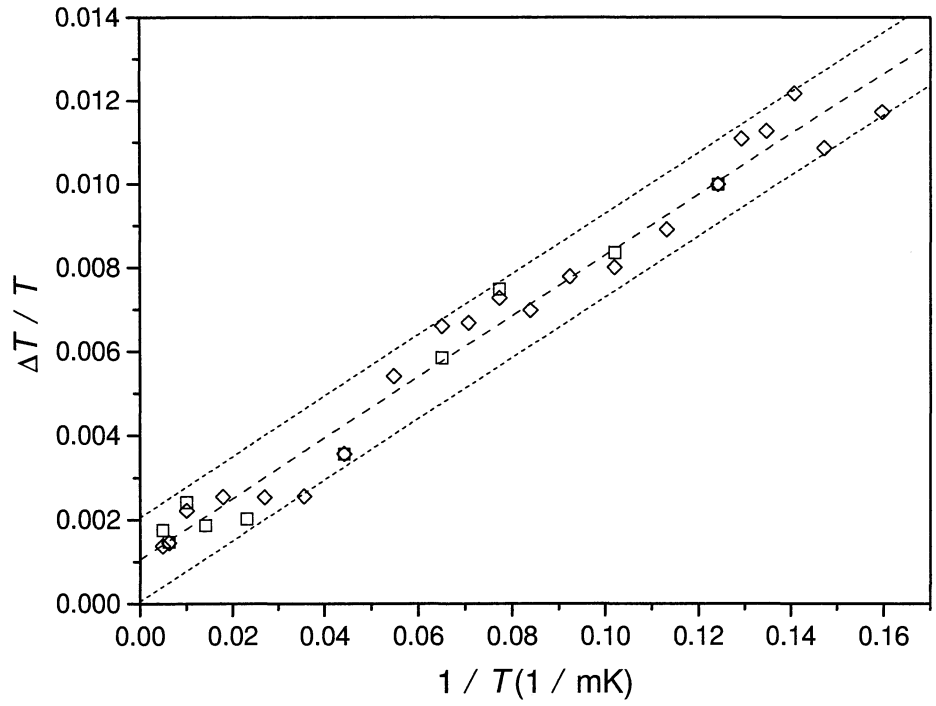

Figure 27. Relative temperature differences between NIST noise (squares) and LCMN thermometer (diamonds) temperatures and PTB-96. The NIST temperatures were taken from [41] and corrected by –0.15% according to [1].

In the temperature range above 500 mK, scale comparisons involve mainly rhodium-iron resistance thermometers that carry the NPL scale T_{XI} [4]. The actual situation is discussed with reference to figure 28 where the results of an intercomparison of rhodium-iron thermometers [45] is shown.

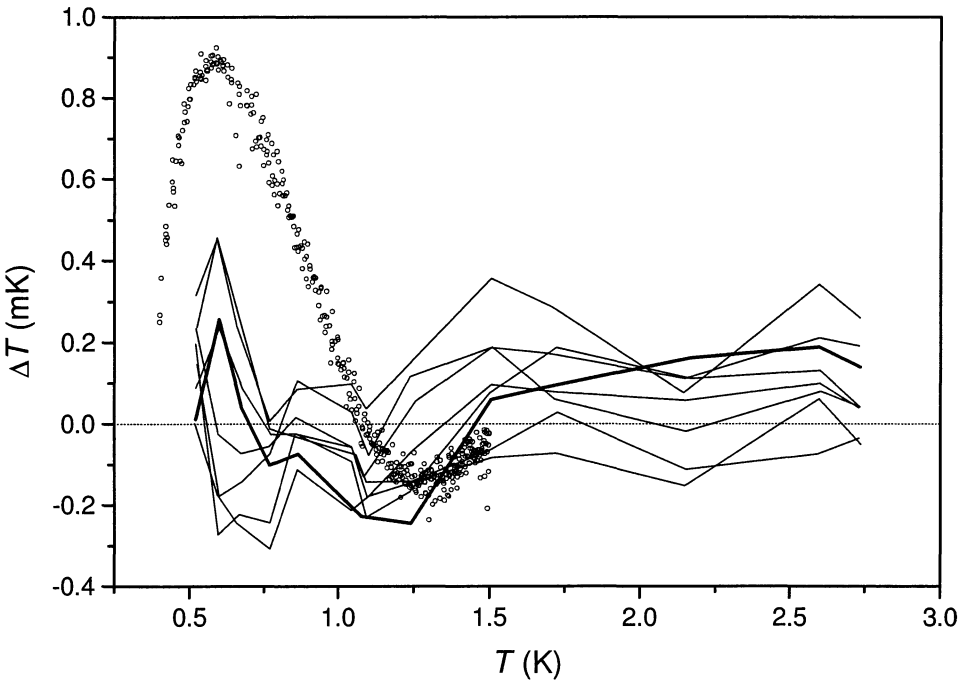

Figure 28. Temperature differences between several rhodium-iron resistance thermometers and T_{XI} (solid lines) after [45]. Thick line denotes resistor B42. Data points are differences between temperatures of B42 and PTB-96.

These thermometers have been re-measured after being in use at different institutions for many years. The temperature differences in the diagram are the deviations of the original calibrations from the actual version of T_{X1} maintained at NPL. At PTB, one of the participating thermometers (B42) was directly compared with the rhodium-iron thermometer whose calibration has been transferred to the ^{3}He melting pressure equation. The data points included in figure 28 represent the temperature differences between the original calibration of B42 and PTB-96. It has to be emphasised that the reference temperature differs for both data sets, but the sets are related by using the same original calibration of B42.

There is agreement between the scales of PTB and NPL near 1.5 K with respect to magnitude and slope, but a systematic deviation is growing towards lower temperatures that reaches an amount by which T_{X1} is high compared to the melting temperatures of at least 0.3 mK ± 0.2 mK at 1 K, and 0.8 mK ± 0.3 mK at 0.6 K.

8. Conclusions

The establishment of the temperature scale PTB-96 between 0.88 mK and 1 K has been described. For practical reasons, its construction was mainly based on magnetic thermometry. The consistency checks presented in this paper have been made at very low temperatures to ensure that the original extrapolation from above 1 K did not progressively deviate from thermodynamic temperature. Confidence in the complete temperature range rests completely on the noise thermometer and is thus of thermodynamic origin. The purpose of using platinum NMR was to identify the admixture of non-thermodynamic parasitic noise voltages and an internal heat leak of the noise thermometer. Both effects severely compromise noise thermometry below 2 mK. The justification for using NMR was the reliability of the Curie law. Thermodynamic consistency with the specific heats of solid and liquid ^{3}He confirmed the shape of PTB-96 below 2.5 mK but failed to establish a firm agreement over a wider temperature range. In view of the arguments collected to clarify the discrepancy, the integrity of the specific heats is doubtful within a few percent.

The structure of PTB-96 offered the opportunity for modifications if measurements of thermodynamic temperatures required a correction. The observed deviations, however, were not sufficiently convincing to justify such changes.

PTB-96 is one of the temperature scales on which the international scale PLTS-2000 is based. For the establishment of PLTS-2000, it was necessary to obtain agreement on the shape of the ^{3}He melting pressure equation. The link to ITS-90 was obtained only outside the range of PTB-96 by an asymptotic junction with T_{X1} [4] at 1.5 K where T_{X1} is supposed to coincide with ITS-90. The temperature scale comparisons made in this paper show that this agreement on the ^{3}He melting temperatures could be reached on a basis between 0.1 mK and 0.5 mK lower than T_{X1} at 1 K. Below this temperature, however, the discrepancies are increasing. Different copies of T_{X1} are probably centred at a deviation of 0.8 mK ±0.3 mK above the melting temperatures at 600 mK, whereas different noise thermometers agree within 0.5 mK at 520 mK. However, the noise thermometers differ by 0.09 mK at 15 mK, where a temperature offset of 0.07 mK is involved. The temperature scales that use extrapolation below 15 mK start with an initial offset of approximately 0.2 mK, and are ending up with 6% discrepancy at 0.9 mK.

Except for the remaining discrepancies with the ^{3}He specific heat near 4 mK, and the temperature offset between the noise thermometer of Soulen *et al.* [44] and that of PTB, no other systematic problems are visible in the complete temperature range. Both discrepancies, however, cannot be resolved without abandoning the Curie law of platinum NMR thermometry.

References

[1] Rusby R.L., Durieux M., Reesink A.L., Hudson R.P., Schuster G., Kühne M., Fogle W.E., Soulen R.J., Adams E.D. 2002, *The Provisional Low Temperature Scale from 0.9 mK to 1 K, PLTS-2000,* J. Low Temp. Phys. **126**, pp 633..642

[2] Schuster G., Hoffmann A., Hechtfischer D. 1996, *^{3}He melting pressure-temperature relation in the range from 1 mK to 1000 mK*, Czech. J. Phys. **46**, pp 481..482

[3] Schuster G., Hoffmann A., Hechtfischer D. 1996, *Temperature scale extension below ITS-90 based on ^{3}He melting pressure*, Doc. CCT/96-25, BIPM, Sèvres, France

[4] Rusby R.L., Swenson C.A. 1980, *A new determination of the helium vapour pressure scales using a CMN magnetic thermometer and the NPL-75 gas thermometer scale*, Metrologia **16**, pp 73..87

[5] Schuster G., Hechtfischer D. 1992, *Extrapolation of ITS-90 to lower temperatures*, Temperature Its measurement and control in science and industry, Vol. **6**, edited by J.F. Schooley, New York, American Institute of Physics, pp 97..100

[6] Hudson R.P., Pfeiffer E.R. 1972, *Temperature scale for cerous magnesium nitrate*, Temperature Its measurement and control in science and industry, Vol. **4**, edited by H.H. Plumb, Pittsburgh, Instrument Society of America, pp 1279..1285

[7] Schuster G. 1992, *Temperature measurement with rhodium-iron resistors below 0.5 K*, Temperature Its measurement and control in science and industry, Vol. **6**, edited by J.F. Schooley, New York, American Institute of Physics, pp 449..453

[8] Schuster G. 1992, *Self-balancing bridge for precise susceptibility thermometry*, Temperature Its measurement and control in science and industry, Vol. **6**, edited by J.F. Schooley, New York, American Institute of Physics, pp 1009..1011

[9] Schuster G., Hoffmann A., Hechtfischer D. 2001, *Realisation of the Temperature scale PLTS-2000 at PTB*, PTB-ThEx-21, ISBN 3-89701-742-3

[10] Schuster G. 1992, *Self-tuning temperature controller for a dilution refrigerator*, Temperature Its measurement and control in science and industry, Vol. **6**, edited by J.F. Schooley, New York, American Institute of Physics, pp 953..954

[11] Hechtfischer D., Schuster G. 2004, *Platinum NMR thermometry below 0.1 K*, PTB-Th-1, ISBN 3-86509-197-0

[12] Hechtfischer, D., Schuster, G. 2003, *The quality of the Curie law in platinum-NMR*, Temperature Its measurement and control in science and industry, Vol. **7**, edited by D.C. Ripple, New York, American Institute of Physics, pp 47..52

[13] Jäger J., Klingenberg G., Schultz W. 1990, *The standard instruments of the PTB for the 5 MPa range of pressure measurement*, PTB-Mitteilungen **100**, pp 429..438

[14] Jäger J. 1994, PTB internal communication, unpublished

[15] Jäger J. 1996, *Ein neues Hauptnormalgerät für Druckmessungen bis 10 MPa,* PTB Annual Report, p 213

[16] Sabuga W. 1996, *Bestimmung der wirksamen Querschnittsflächen von neuen 5-cm²-Gas- und -Öl-Kolbenzylindersystemen,* PTB Annual Report, pp 213..214

[17] Jäger J., Schultz W. 1997, *Druckvergleichsmessungen zwischen einem Quecksilber- und einem Kolbenmanometer bei Überdrücken bis 2.2 MPa,* PTB Annual Report, pp 207..208

[18] Jäger J., Sabuga W., Waßmann D. 1997, *Verbesserung bei der Realisierung der Druckskala im Messbereich bis 10 MPa,* PTB Annual Report, pp 208..209

[19] Ban S., Jäger J., Legras J.C., Matilla C., Rantanen M., Steindl D. 2002, *Report on the results of measurements performed in the period from May 1994 to October 1995 in the framework of the EUROMET Project 305*, BIPM key comparison database, www.bipm.fr

[20] Jäger J., Sabuga W., Waßmann D. 1999, *Piston-cylinder assemblies of 5 cm^2 cross-sectional area used in an oil-operated primary pressure balance standard for the 10 MPa range*, Metrologia **36**, pp 541..544

[21] Bauer H., Jäger J. 1980, *International comparison of pressure balance standards over the 1 MPa to 10 MPa range*, Metrologia **16**, pp 111..115

[22] Klingenberg G., Legras J.C. 1993/94, *Bilateral comparative pressure measurements of the LNE and the PTB using 10 cm^2 piston-cylinder assemblies*, Metrologia **30**, pp 603..606

[23] Legras J.C., Sabuga W., Molinar G.F., Schmidt J.W. 1999, *CCM key comparison in the pressure range 50 kPa to 1000 kPa (gas medium, gauge mode) Phase A2: Pressure measurements*, Metrologia **36**, pp 663..668

[24] Gorobey V., Kiselev Yu., Jäger J., Sabuga W., Farar P., Faltus Z. 1999, *Comparison of the national pressure standards of the Russian Federation (VNIIM), Germany (PTB) and Slovakia (SMU) in the range 1 MPa to 3 MPa*, Metrologia **36**, pp 651..655

[25] Colwell J.H., Fogle W.E., Soulen R.J. 1992, *The ^{3}He melting curve thermometer as a universal temperature transfer standard*, Temperature Its measurement and control in science and industry, Vol. **6**, edited by J.F.Schooley, New York, American Institute of Physics, pp 101..106
[26] Hechtfischer D., Schuster G. 1992, *Parasitic temperature-dependence in platinum NMR thermometry*, Temperature Its measurement and control in science and industry, Vol. **6**, edited by. J.F. Schooley, New York, American Institute of Physics, pp 107..111
[27] Hoffmann A., Schuster G., Engert J., *Noise thermometry at ultra-low temperatures*, PTB-Report, to be published.
[28] Buck W., Hechtfischer D., Hoffmann A. 1990, *A nuclear demagnetisation cryostat for thermometry*, Physica B **165&166**, pp. 49..50
[29] Bandler S.R., Enss C., Schönefeld J., Seidel G.M. 1996, *Study of paramagnetic ions in metals for use in cryogenic particle detection*, Czech. J. Phys. **46**, pp 2889-2890
[30] Hechtfischer D., Schuster G. 2003, *Simplifying the realisation of PLTS-2000 with the tungsten superconductive transition*, Temperature Its measurement and control in science and industry, Vol. **7**, edited by D.C. Ripple, New York, American Institute of Physics, pp 149..154
[31] Fellmuth B., Hechtfischer D., Hoffmann A. 2003 *PTB-96: The Ultra-low temperature scale of PTB*, Temperature Its measurement and control in science and industry, Vol. **7**, edited by D.C. Ripple, New York, American Institute of Physics, pp 71..76
[32] Greywall D.S. 1986, *^{3}He specific heat and thermometry at millikelvin temperatures*, Phys. Rev. B **33**, pp 7520..7538
[33] Greywall D.S., Busch P.A. 1987, *Nuclear specific heat of bcc ^{3}He near the magnetic ordering transitions*, Phys. Rev. B **36**, pp 6853..6870
[34] Reesink A.L. 2001, *Thermodynamic calculation of ^{4}He and ^{3}He saturated vapour pressures and ^{3}He melting pressures*, PhD Thesis, University of Leiden
[35] Halperin W.P., Rasmussen F.B., Archie C.N. and Richardson R.C. 1978, *Properties of melting 3He: Specific heat, entropy, latent heat, and temperature*, J. Low. Temp. Phys. **31**, pp 617..698
[36] Fukuyama H., Ishimoto H., Tazaki T., Ogawa S. 1987, *^{3}He melting curve below 15 mK*, Phys. Rev. B **36**, pp 8921..8924
[37] Ni W., Xia J.S., Adams E.D., Haskins P.S., McKisson J.E. 1995, *^{3}He melting pressure temperature scale below 25 mK*, J. Low Temp. Phys. **99**, pp 167..183
[38] Grilly E. R. 1971, *Pressure-volume-temperature relations in liquid and solid ^{3}He*, J. Low Temp. Phys. **4**, pp 615..635
[39] Greywall D.S. 1985, *^{3}He melting-curve thermometry at millikelvin temperatures*, Phys. Rev. B **31**, pp 2675..2683
[40] Schuster G., Hechtfischer D., Buck W., Hoffmann A. 1990, *Consistency of low temperature scales and the temperature of the ^{3}He melting pressure minimum*, Physica B **165 &166**, pp 31..32
[41] Fogle W. E., Soulen R. J. and Colwell J. H. 1992, *ITS-90 below 1K: How accurate is it?*, Temperature Its measurement and control in science and industry, Vol. **6**, edited by. J.F. Schooley, New York, American Institute of Physics, pp 85..90
[42] Bremer J. and Durieux M. 1992, *Noise thermometry, ^{3}He melting pressures and superconducting transition temperatures between 0.4 K and 0.09 K,* Temperature Its measurement and control in science and industry, Vol. **6**, edited by. J.F. Schooley, New York, American Institute of Physics, pp 15..20
[43] Fogle W.E., Soulen R.J. 1998, *The NIST millikelvin temperature scale*, Proceedings of the CCT Workshop 'Toward an International Temperature Scale from 0.65 K to 1 mK', edited by R.L. Rusby and P. Mohandas, Leiden, pp 13..19
[44] Soulen R.J., Fogle W.E., Colwell J.H. 1994, *Measurements of absolute temperature below 0.75 K using a Josephson-junction noise thermometer*, J. Low Temp. Phys. **94**, pp 385..487
[45] Head D.I., Rusby R.L. 1993, *A EUROMET intercomparison of rhodium-iron resistance thermometers*, Doc. CCT/93-15, BIPM, Sèvres, France,